Climate Dynamics
https://doi.org/10.1007/s00382-020-05209-2

Improved historical simulation by enhancing moist physical parameterizations in the climate system model NESM3.0

Young-Min Yang[1] · Bin Wang[1,2] · Jian Cao[1] · Libin Ma[3] · Juan Li[1]

Received: 9 August 2019 / Accepted: 12 March 2020

Abstract
The third version of the Nanjing University of Information Science and Technology (NUIST) Earth System Model (NESM3.0) has been recently developed for sub-seasonal to seasonal climate prediction and projection of future climate change. This requires realistic simulation of both internal modes of climate variability and global energy balance and climate sensitivity. In the historical experiments based on the coupled model intercomparison project (CMIP6) forcings, the original version of NESM3.0 does a reasonably good job in capturing warming trends and climate sensitivity to external forcing, but not in simulating climatology and climate variability. For our project we modified the deep and shallow convective scheme, cloud cover, and cloud microphysics in the atmospheric model. We then conducted hundreds of experiments to test the results in the fully coupled model with comprehensive metrics to ensure that any individual targeted improvement does not affect the overall performance. The modifications in moist physics improved the model's climatology and internal variability significantly without degrading global energy balance and climate sensitivity. The key was to reduce the model's warm sea surface temperature (SST) bias and associated excessive precipitation bias in the tropics by reducing convective precipitation and increasing large-scale stable precipitation. This effort leads to more realistic simulation of the zonal mean circulation and temperature structure, global monsoon, and ocean salinity. The El Niño Southern Oscillation (ENSO) simulation was improved by reducing wind stress biases associated with ENSO in the central and eastern Pacific. Better ENSO leads to better teleconnection in mid-latitudes, particularly over the North Pacific and Atlantic Ocean. The eastward propagation of the Madden–Julian Oscillation (MJO) was significantly improved by enhancing the interaction between the boundary layer and lower tropospheric heating. These results suggest that improvement in moist physical parameterizations is an effective way to improve simulation of climatology and major modes of internal variability without degrading the global energy balance and climate sensitivity in the historical run.

Keywords Climate model · CMIP6 · Historical simulation · Convective parameterization · Climate variability · Cloud microphysics · Shallow convection

1 Introduction

Climate modeling is an essential tool to understand dominant mechanisms of climate variability, conduct climate prediction, and project future changes of climate induced by greenhouse gases, aerosol and other forcings. Improving climate models is, therefore, one of the major endeavors in climate research. Since 1995, the World Climate Research Programme (WCRP) has organized coupled model intercomparison projects (CMIPs; Meehl et al. 2000). The CMIP data were used to find common problems in models and understand scientific issues related with current climate variability and climate change, and provide information for

✉ Bin Wang
wangbin@hawaii.edu

[1] Key Laboratory of Meteorological Disaster, Ministry of Education/International Joint Research Laboratory on Climate and Environment Change/Collaborative Innovation Center on Forecast and Evaluation of Meteorological Disasters, Nanjing University of Information Science and Technology, Nanjing 210044, China

[2] Department of Atmospheric Sciences and International Pacific Research Center, University of Hawaii, Honolulu, HI 96822, USA

[3] State Key Laboratory of Severe Weather, Chinese Academy of Meteorological Sciences, Beijing 100081, China

Published online: 21 March 2020

human society to adapt to Earth's changing environmental system (Taylor et al. 2012).

Many previous studies evaluated and investigated systematic biases in CMIP5 participant models. Kumar et al. (2013) showed that the multi-model ensemble (MME) of CMIP5 models captures observed global and temperature trends from 1930 to 2004 but fails to reproduce local/regional temperature and precipitation trends. Our evaluation showed that the sea surface temperature (SST) trend of CMIP5 MME for the period of 1979–2004 (1.43 °C/100 year) is larger than observed (1.13 °C/100 year). For land temperature, the trends of CMIP 5 MME (3.20 °C/100 year) are much larger than observed (2.48 °C/100 year), suggesting that the CMIP5 models have difficulty predicting future changes in land temperature. Li and Xie (2012) discussed the strong cold SST bias in the equatorial Pacific and the double intertropical convergence zone (ITCZ) problem, where unobserved excessive precipitation occurs. They suggested that the double ITCZ problem results from tropical ocean–atmosphere interaction (e.g., Bjerknes feedback). Lee et al. (2010) showed that the MME underestimates precipitation over the eastern Indian Ocean, equatorial western Pacific, and tropical Brazil, and overestimates over the Maritime Continent and the Philippines. They also found that the MME captures global monsoon precipitation well except over the western North Pacific-East Asia. Chen et al. (2017) evaluated the ENSO behavior of CMIP5 MME and showed that CMIP5 models have difficulty in simulating El Niño characteristics and seasonal phase locking. On the other hand, Lee and Black (2013) showed that many CMIP5 models reproduce North Atlantic Oscillation (NAO)-like and Pacific-North American (PNA)-like patterns well. Many CMIP5 models failed to simulate the eastward propagation of Madden–Julian Oscillation (MJO) convection (Hung et al. 2013) and Arctic sea ice thickness, although they did a good job of capturing the climatology of Arctic sea ice extent (Shu et al. 2015). Moreover, trends of Artic sea ice in CMIP5 models are smaller than observations (Stroeve et al. 2012).

The third generation of the Nanjing University Information Science and Technology (NUIST) Earth System Model (hereafter, NESM3.0) (Cao et al. 2018; Yang et al. 2018; Yang and Wang 2019) was developed recently. The fully coupled NESM3.0 consists of atmosphere, land, ocean and sea ice model components. It was established to conduct sub-seasonal to decadal climate prediction, simulate past and future climate change, and study various mechanisms and processes responsible for climate variability. The performance of NESM3.0 was examined in pre-industrial control runs (Cao et al. 2018) and evaluated for the present Asian-Australian Monsoon (Li et al. 2018). It was also used to conduct seasonal prediction in the East Asia region (Yang et al. 2018) and investigate key processes and associated parameterizations for enhanced MJO simulations (Yang and Wang 2019; Yang et al. 2019b). The model was also utilized to find a dominant mechanism for northward propagation of intra-seasonal summer precipitation in the eastern India Ocean (Yang et al. 2019a). It was also used to study multi-decadal relationship between Pacific and North Atlantic ocean (Yang et al. 2019c).

We conducted the historical simulation with an earlier version of NESM3.0 and evaluated its performance using a comprehensive diagnostic tool (e.g., Li et al. 2018). The earlier model can produce a reasonably realistic temporal evolution of global surface temperature under external forcings (e.g., greenhouse gases) but overestimates surface temperature warming for the entire period of the historical run and the trend of recent warming from 1979 to 2005. The warm biases in SST induce wet biases in precipitation, contributing to the biases in the vertical profile of climatological temperature and circulation. The simulated intraseasonal oscillation does not propagate eastward, the interannual variability of SST in the equatorial Pacific is overestimated, and the ENSO phase locking failed. The model also poorly simulated the Pacific-North American teleconnection pattern.

Here we report our efforts to improve the historical run based on CMIP6 protocol by modifying physical parameterizations. We explain how the modified parameterizations affect temporal evolution of global surface air temperature, some aspects of climatology, and climate variability. Section 2 describes the model, data, and strategy and methodology used to improve model parameterizations. Section 3 describes the original model's deficiencies and modified parameterizations. Section 4 discusses how the modified parameterizations improved historical simulation based on diagnostic analysis and the last section presents a summary.

2 Data and methodology for model improvements

2.1 The NESM model and data used for evaluation

We use the third version of the Nanjing University of Information Science and Technology (NUIST) Earth System Model (NESM3.0). The NESM3.0 is composed of: atmosphere (ECHAM v6.3; Stevens et al. 2013); ocean (NEMO v3.4; Madec et al. 2008); sea ice model (CICE); and land model (JSBACH, Raddatz et al. 2007). The model is fully coupled with each component by a coupler (OASIS3-MCT_3.0; Valcke et al. 2013). The resolution of the atmosphere model is T63L47. The ocean model has a resolution of 1° grid with the meridional resolution refined to 1/3° over the equatorial region. It has 46 vertical layers with the first 15 layers at the top 100 meters. The ECHAM v6.3 and JSBACH model are originally developed at the Max Planck Institute (Stevens et al. 2013). The convective

parameterization is based on the mass-flux framework developed by Tiedtke (1989) and further modified by Nordeng (1994) (TDK, hereafter). The stratiform cloud scheme contains prognostic equations for the vapor, liquid, and ice phase of water, a cloud microphysical scheme, and a diagnostic cloud cover scheme. A detailed description of the model is documented in Cao et al. (2018).

Two sets of historical runs were compared to evaluate the impact of the modified parameterizations: (1) simulations without modified parameterizations (CTL); and (2) model simulations with the modified parameterizations (MOD). For all experiments, the model is fully coupled and integrated from 1850 to 2014 using the external forcing (greenhouse gases, solar constant, aerosol concentration, ozone, etc.) based on the CMIP6 protocols. The 25-year data (1979–2005) were used to analyze the model climatology and variability and compare with CMIP5 models' performance. The initial condition for the integration was obtained from a pre-industrial run based on the CMIP6 protocols.

The National Centers for Environmental Prediction-Department of Energy (NCEP-DOE) Reanalysis II data (Kanamitsu et al. 2002) were used to represent observed winds, air temperature and geopotential heights. The observed precipitation data were derived from the Global Precipitation Climatology Project (GPCP) daily data (Adler et al. 2003). For monthly mean sea surface temperature (SST) we used the National Oceanic and Atmospheric Administration Extended Reconstructed SST (ERSST) version 4 data (Huang et al. 2016). The European Center for Medium-Range Weather Forecast (ECMWF) Reanalysis (ERA) Interim data were used to calculate circulation anomalies associated the MJO (Dee et al. 2011). The ocean temperature and salinity derived from the ECMWF ocean reanalysis and ocean heat content datasets (ORAS4) were used as observations (Balmaseda et al. 2013).

2.2 Strategy and methodology for improving model parameterizations

Our principal strategy is to always use coupled model experiments to assess the impacts of model's parameterization changes on model's simulation. This is because any change made in a component model may affect the coupled model climatology and variability. We also use comprehensive metrics to evaluate the model's performance and avoid using only specific metrics for one aspect of the model performance. This is because a change in parameterization targeted for a specific improvement may degrade the model's performance in other aspects. An acceptable modification of parameters should improve overall performance. For this purpose, we designed metrics that include 150 fields to evaluate: global energy and water balance; climate sensitivity; climatology of the atmosphere, ocean, sea ice, and land; and major modes of climate variability. Hundreds of sensitivity experiments were conducted to test the results of modified parameterizations to model simulations.

3 Improvement of model physical parameterizations

3.1 The original model's deficiencies in the historical simulation and possible causes

One of the major problems in the CTL simulation is the warm SST bias in the tropics, which influences both mean precipitation and global monsoon, and also large-scale circulations. When we reduce the amount of solar radiation downward by increasing cloudiness, warm SST biases were significantly reduced but the precipitation climatology and monsoon simulations were little improved, suggesting that moist physics processes need to be modified. The model simulated total precipitation is mainly produced by convective precipitation, particularly over the tropics, suggesting that modifying convective parameterization may be a key process to improve precipitation climatology and monsoon simulations. Another problem in the original model is evident in the ENSO simulation. The CTL simulates excessively strong interannual variances in the equatorial Pacific SST. In the model, the minimum SST variance occurs in late summer rather than in spring as in observation. We hypothesize that the strong variability may result from excessive response of SST anomalies to zonal wind stress and precipitation heating, and/or results from the strong zonal gradients of the mean-state SST by the warm SST biases in the western Pacific. It is known that the interannual variability is sensitive to convective parameterizations. Watanabe et al. (2011) showed that increasing the entrainment rate in a convective scheme might decrease the SST variability by reducing the Bjerknes feedback. Kim et al. (2011) showed that a weak moisture trigger reduces the SST variability by westward shift of the zonal wind stress anomalies. Thus, the key processes for decreasing ENSO amplitude may be reducing the precipitation and zonal wind stress anomalies associated with SST anomalies by modifying convective parameterization schemes. The lack of ENSO phase-locking to annual cycle may be improved by suppressing convection, which may shift the ENSO locking timing from summer to spring (Ham et al. 2013). The PNA pattern is strongly influenced by ENSO. The main problem with the ENSO simulation in the CTL is the westward extension of interannual variability, which may be reduced by modification of a convective scheme.

The MJO convection in the earlier version of the model does not propagate eastward. From the trio-interaction theory (Wang et al. 2016) and global climate models'

diagnostics (Wang and Lee 2017), the boundary layer moisture convergence feedback plays a key role in driving eastward propagation of the MJO and enhancing the interaction between the boundary layer moisture convergence (BLMC). Lower tropospheric heating is critical for realistic MJO simulation (Zhang and Song 2009; Yang and Wang 2019; Wang et al. 2018). Therefore, suppressing deep convection and enhancing shallow convection may improve the eastward propagation of MJO precipitation by enhancing the interaction between lower tropospheric heating and BLMC.

Over the land surface, there are warm biases in the Amazon basin, India, Central Africa and Asia. The biases may affect land precipitation and snow depth in Siberia, which may affect the trend of surface temperature. The warm biases on land are partly attributed to excess downward solar radiation, suggesting that increased cloudiness may be helpful for reducing the warm biases. In the Arctic Ocean, sea ice is over-melted, which may be due to inadequate sea ice melting parameterizations used in the albedo scheme. Changing the sea ice albedo scheme may be a simple way to reduce excessive sea ice melting without degrading the radiative balance in other regions. In the Antarctic, sea ice is also over-melted, which is mainly due to warm SST biases in the Southern Ocean. The insufficient super-cooled cloud water and cloud cover may induce the warm SST biases near the Antarctic region.

Given the problems with the early version, we need to improve the model's capacity to simulate both reasonable temporal evolution of surface temperature and realistic climatology and variability without degrading global energy and water balance.

3.2 Major modifications and tunings made to the parameterization schemes

We modified the convective parameterization, cloud microphysics, and cloud cover scheme in the NESM3.0. We added a boundary depth-dependent convective trigger to the convective scheme (hereafter 'TRG'; Yang et al. 2018; Yang and Wang 2019). This trigger is modified from the Tokioka constraint Tiedtke et al. (1988). The Tokioka constraint was implemented in the Arakawa–Schubert scheme, which allows generation of multiple clouds in a grid box. This constraint turns off deep convective cloud and allows shallow clouds when PBL depth is relatively shallow. In this study, we implemented the Tokioka constraint in the TDK scheme with a single updraft. However, when original Tokioka constraint was added, the deep or middle cloud tends to be suppressed too frequently. The suppressed deep cloud accumulates convective instability that tends to be removed by large-scale condensation, which increases total cloudiness. The increased cloudiness leads to unexpected biases in the simulated climatological SST pattern and affect the global energy balance, particularly in coupled models. In order to reduce degrading the climatology by the original Tokioka constraint in the coupled model, we applied different criteria to control the onset of each cloud type. The criteria for deep and middle convection are relaxed compared to that for shallow convection, so that more deep clouds can be generated when compared to the same criteria for all cloud types.

$$\varepsilon_{\min} = \frac{a_i}{h}, \quad \begin{array}{ll} \text{convection turns off,} & \text{if } \varepsilon \le \varepsilon_{\min} \\ \text{convection turns on,} & \text{if } \varepsilon > \varepsilon_{\min} \end{array} \tag{1}$$

where h refers to the BL depth, $\varepsilon_{\min}$ is minimum entrainment rate, i is cloud type (deep, midlevel and shallow convection), and a_i is a constant. This trigger turns off convection when the BL depth is relatively shallow. We used different constants for shallow (a = 0.015), midlevel (a = 0.010), and deep convection (a = 0.005), which effectively reduced the change in cloudiness by the trigger function, improving simulated precipitation without degrading the radiative energy balance. In the western Pacific, when convection is suppressed, the convective instability tends to be largely removed by large-scale condensation because the relative humidity is relatively high. In the eastern Pacific, however, the accumulated convective instability is partly (small portion) consumed by large-scale condensation (e.g., Fig. 4a).

Second, we added a bottom-heavy diffusivity in the shallow convection scheme (SHC) (Yang and Wang 2019), which was modified from Tiedtke et al. (1988). This scheme is described by the following diffusive terms for large-scale (grid mean) dry static energy S and specific humidity q (Tiedtke et al. 1988).

$$\frac{\partial \bar{s}}{\partial t} = \frac{1}{\bar{\rho}} \frac{\partial}{\partial z} \left\{ \bar{\rho} K \frac{\partial}{\partial z} \left(\bar{s} - L\bar{l} \right) \right\} \tag{2}$$

$$\frac{\partial \bar{q}}{\partial t} = \frac{1}{\bar{\rho}} \frac{\partial}{\partial z} \left\{ \bar{\rho} K \frac{\partial}{\partial z} \left(\bar{q} + \bar{l} \right) \right\} \tag{3}$$

where l denotes cloud liquid water content, ρ the air density, L the latent heat, t the time and z the height. The coefficient K is the eddy diffusivity, which is a prescribed function of height or pressure. The main difference in the shallow convection scheme used in this study and the earlier scheme (Tiedtke et al. 1988) is that our shallow convection scheme implements a specific vertical profile of vertical mixing below 600 hPa. In the earlier NESM3.0, vertical mixing in the lower troposphere is relatively weak, resulting in insufficient upward transport of moisture and diabatic heating, particularly in the tropics. The new shallow convection scheme has a specific vertical profile for turbulent mixing. The vertical mixing near 925 hPa is heavy and then gradually

reduces to 0 at 600 hPa. When we implemented this shallow convection to the earlier NESM3.0, it effectively enhanced shallow convection in the lower troposphere. It is known that the lower tropospheric heating to the east of MJO deep convection may play a role in improving MJO simulation (Wang et al. 2018; Yang and Wang 2019). Wang et al. (2018) showed that the climate models with better lower tropospheric heating to the east of the convection center has better MJO propagation skill. The shallow convective scheme used in this study may produce better MJO simulation if lower tropospheric heating is enhanced.

Third, we changed the conversion rate from convective cloud water to rain in the convective scheme. This change reduces the amount of convective precipitation and increases detrainment of remaining cloud water in the updraft to the ambient air, which leads to enhanced stratiform cloud. In the convective scheme, we change the conversion rate of cloud water to rain (Gp). This process is assumed to be proportional to liquid water in cloud (l) and empirical function (K), which varies with height (Tiedtke 1989).

$$\mathrm{Gp} = \mathrm{K(z)l} \tag{4}$$

where l is liquid water content in the cloud and K(z) is constant at height, 2×10^{-3} h. We reduced this value by 30%, which is in a normal range of observed variability (Yanai et al. 1973). This parameter changes the amount of convective precipitation and also the downdraft and re-evaporation below cloud-base, which can affect the associated surface circulation and temperature.

Fourth, the entrainment rates in deep and shallow clouds were increased over the ocean region. An increasing entrainment rate tends to suppress deep convection by enhancing mixing with relatively dry and cold environmental air. The convective cloud is calculated twice in the convective scheme. At the first iteration, the entrainment rate is estimated using convective velocity and buoyancy of convective clouds (Möbis and Stevens 2012) and the cloud top is determined by the entrainment rate in the original convective scheme. We modified the formula for entrainment rate as follows: an entrainment rate (ε) is parameterized based on buoyancy (B_u) and grid-mean humidity (RH) based on Kim and Kang (2012).

$$\varepsilon = a_0 \times c_\varepsilon \times B_u, \quad c_\varepsilon = \frac{1}{\mathrm{RH}} \tag{5}$$

where, c_ε and a_0 are conversion factors of grid-mean humidity and buoyancy on entrainment rate, respectively. When RH is high (> 99%), c_ε is fixed at $1.e^{-1}$. For low RH (< 10%), c_ε is 10. The maximum (minimum) value of the entrainment rate is constrained to $1.e^{-2}$ ($1.e^{-6}$) m^{-1}. If the depth of convective cloud between the level of neutral buoyancy and lift condensation level is larger (smaller) than 200 hPa, deep (shallow) convection is assumed for the second iteration. At the second iteration, deep and shallow convection use different entrainment profiles. We increase the entrainment profiles to 1.78×10^{-4} m^{-1} (for deep convection) and 3.5×10^{-3} m^{-1} (for shallow convection), respectively.

We also tuned the cloud cover scheme and cloud microphysics in stratiform cloud to reduce biases in the global energy balance (e.g., the short/long wave radiation at the top of atmosphere and sea surface). The modified convective parameterizations described above tend to suppress convective precipitation and increase stratiform precipitation, which induces excessive cloudiness. To prevent the global energy balance being degraded by the modified convective parameterizations, we increased the autoconversion rate from cloud water to rain and accretion from cloud ice to snow in the stratiform cloud processes. Increasing the autoconversion and accretion rates reduces the cloud optical depth and then increases downward solar radiation, which contributes to a better global radiative budget for the modified parameterizations. Beheng (1994) showed that the ranges of autoconvection and accretion rate are relatively large. The ratio of maximum to minimum value is about 1×10^3, which means the values for accretion and autoconversion rate is largely uncertain. Previous studies (Beard and Pruppacher 1969; Beard 1976; Langleben 1954) show that the range of terminal velocity of water drop (snow) is from 1.0 to 4.0 m/s (0.4–1.2 m/s), suggesting that the modified terminal velocity used in this study is within the observed range. Also, Kang et al. (2014) shows that terminal velocity reduced by 50% may induce better-simulated precipitation. In this study, we doubled the autoconversion and accretion rates. We also decreased the terminal velocity for snow and rainwater to 50% of the original values. The decreased terminal velocity makes snow and rain stay in the air for a longer time, increasing the amount of the conversion from cloud water (ice) to rain (snow). Note that the modified parameterizations do not appreciably change global precipitation.

In order to reduce the warming bias in surface temperature (Fig. 5a), we decreased the entrainment rate for deep convection over land region to enhance deep convection, which could reduce the downward solar radiation by increasing cloudiness. The enhanced deep convection over land region may increase convective precipitation and thus increase soil moisture and evaporation, leading to further cooling of the surface. To reduce excessive sea ice in the Arctic region, we modified a coefficient of "melting pond parameterization" in the sea ice model, which affects sea ice albedo in both the Arctic and Antarctic regions. During the melting season, the snow and sea ice surface melt and form ponds. The albedo of pond-covered ice is measured from 0.1 to 0.5. This value is lower than that of bare ice (generally 0.6–0.65) (Perovich and Tucker 1997; Perovich et al. 2002). Therefore, melt ponds significantly affect the

area-averaged albedo. In the original sea ice model, the melting pond parameterization was included implicitly by adjusting sea ice and snow albedo based on surface condition. We reduced a coefficient from melting pond parameterization, which determines melt pond volume, up to 20%. This decreases sea ice albedo during the melting season and thus sea ice could be reduced. Note that the change in sea ice albedo may not improve its annual cycle.

4 Improved historical simulations and reasons for improvements

4.1 Response of the global mean surface air temperature to external forcings

Figure 1 shows time evolutions of the global mean SST and 2 m air temperature over land from historical simulations and observation. The CTL produces warm global SST and 2 m land temperature during the historical simulation period, however, the MOD reduces the warm biases significantly. During the period from 1850 to 2005, the CTL overestimates the trends of SST (0.45 °C/100 year) and 2 m land air temperature (0.92 °C/100 year). The MOD reduces the trends of SST (0.40 °C/100 year) and 2 m land temperature (0.82 °C/100 year) but they are still slightly higher than observed. Figure 1c shows the time series of global surface temperature. The CTL produces warm bias in global surface temperature during the historical simulation period. But the MOD reduced the bias and improved the simulation. The observation also shows the cooling effects induced by volcanic eruptions (e.g., 1902, 1963 and 1991). The CTL and MOD captured these cooling episodes and there is no significant change between the two model versions.

Figure 2 represents time series of the global net radiation at the top of the atmosphere. The CTL produces negative energy balance before 1975 and positive after 1976. The CTL show a significant increasing trend with 1.7 W m^{-2}/100 year during 1900–2005, which is much larger than the multi-model ensemble (MME) of the CMIP5

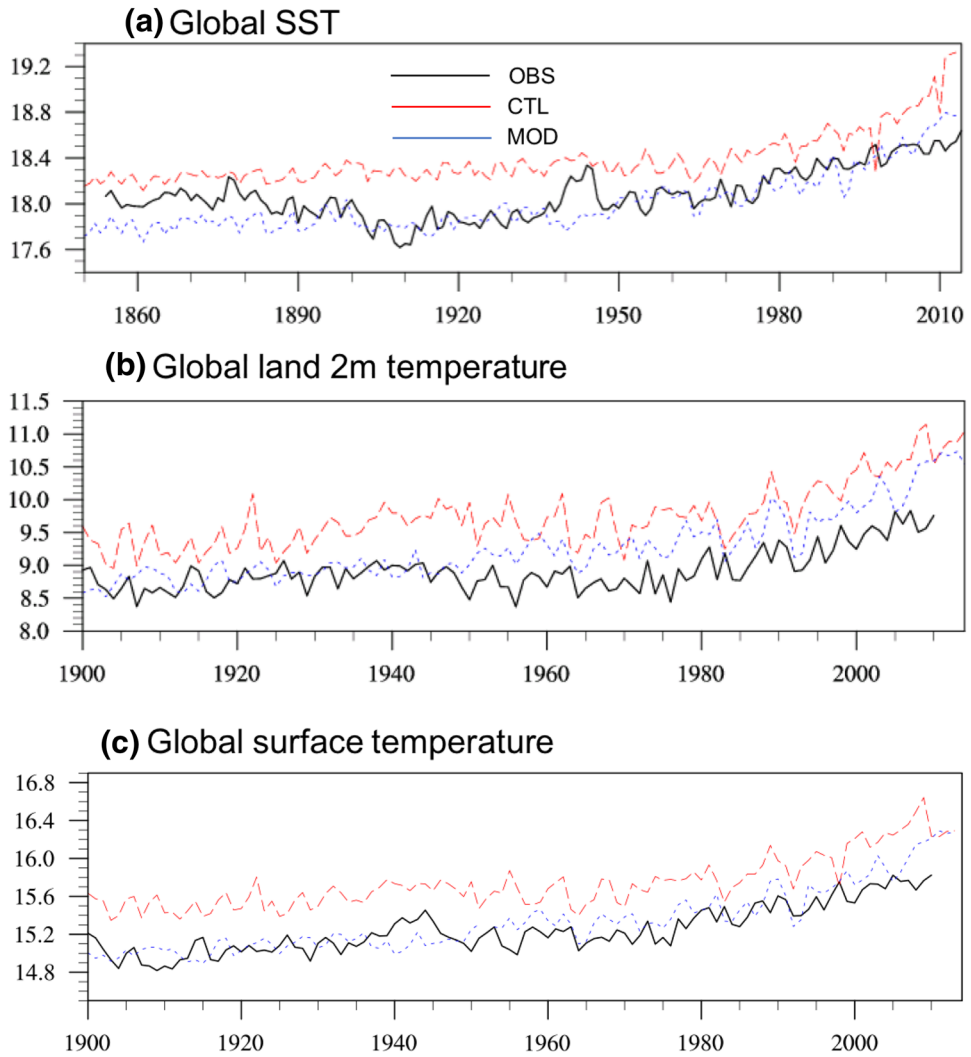

Fig. 1 Time evolution of **a** global mean SST, **b** land 2 m air temperature and **c** global surface temperature (90° S–90° N) from observation and models. Annual mean data are used. Global surface temperature is defined as combined global SST and land 2 m air temperature based on an area-weighting method

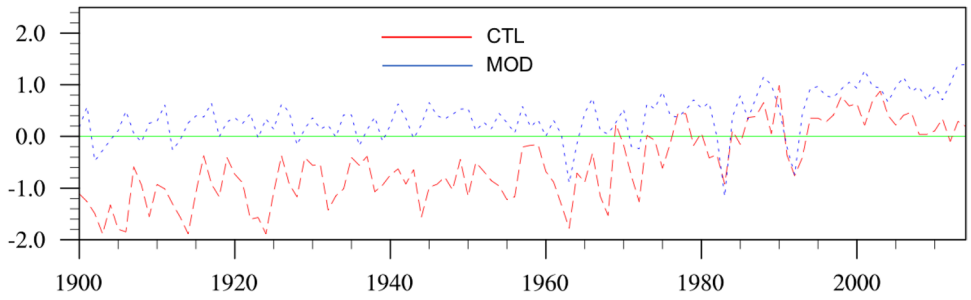

Fig. 2 Time evolution of (a) global mean net radiation at top of the atmosphere (90° S–90° N) from models. Annual mean data are used

models (0.51 W m^{-2}/100 year). However, the MOD produces positive energy balance with relatively small magnitude and an increasing trend after 1965. An increasing trend during 1900–2005 is about 0.6 W m^{-2}/100 year closer to CMIP5 MME.

The improvement is due to the increased cloudiness by the modified convective scheme (e.g., convective trigger, increased entrainment rate) that cools the tropics, and thus reduces the global mean SST biases. There is no clear reason for the reduced trends in global SST during 1850–2004. One possible reason is the improved interdecadal Pacific oscillation (IPO) due to enhanced mean state. From 1998, the IPO is in a negative phase, which slows down the global warming trend (Meehl et al. 2014).

4.2 Improved climatology

Figure 3 compares spatial patterns of the annual mean SST (1979–2005) from observation and model biases. The CTL produces a warm SST bias in the tropics and Southern Ocean, and cold biases in the North Atlantic and North Pacific. The maximum cold bias in the North Atlantic reaches 5°–6 °C. The MOD simulation improved horizontal patterns of SST by reducing those biases in the tropics, Southern Ocean, and the Antarctic regions, but produced more cold biases in the Ross and Amundsen Sea. The cold biases in the North Atlantic Ocean decreased but were still much colder than observations. The improved lower SSTs in the Indian Ocean and western Pacific are attributed to suppressed convective precipitation by the modified convective scheme. Figure 4a shows the ratio of the convective to the total precipitation from the CTL and MOD. Compared to CTL, the ratio in MOD is significantly reduced over most tropical ocean regions except the western North Pacific. It suggests that, in MOD, convection is suppressed, while large-scale condensation is enhanced. Figure 4b shows the difference in the total cloud cover between CTL and MOD (MOD minus CTL). In tropical oceans, there is an increase of total cloud cover, which is consistent with the horizontal pattern of the suppressed convective precipitation. This suggests that the increase in total cloud cover may be due to reduced convection and increased large-scale precipitation. The increase in cloud cover reduces downward shortwave radiation and net surface radiation (Fig. 4c), inducing a decrease in SST. There is a significant decrease in cloud cover in the western Pacific and eastern Indian Ocean, which is consistent with the change in SST in MOD. The change in SST in the North Atlantic may be mainly due to the change in sea ice–ocean interaction by the modified sea ice albedo scheme. The horizontal patterns of SST biases in the MOD are quite similar to the MME of CMIP5 except in the North Atlantic, Ross, and Amundsen Seas (Fig. 2d). Figure 2e shows that the range of the normalized root mean square error (NRMSE) of CMIP5 models is from 0.085 to 0.14 but the pattern correlations have a small spread, indicating that CMIP5 models can generally capture horizontal pattern of SST but that the magnitudes of biases are largely different.

Figure 5 shows the biases of mean 2 m temperature over land in the CTL and MOD. The CTL has strong warm biases in the central Africa and Amazon region but the MOD reduced those warm biases. However, the warm biases in North America were not reduced.

Figure 6 shows that the CTL overestimates precipitation in the western Pacific, ITCZ, South Pacific Convergence Zone (SPCZ) and tropical Atlantic Ocean, as well as in West Africa. The strong precipitation seen in the southeastern Pacific reflects the typical "double ITCZ" problem. Compared to CTL, the MOD improved the horizontal pattern of precipitation and significantly reduced the wet bias in the western Pacific, ITCZ, and SPCZ. This is attributed to the reduced SST biases and suppressed convection due to the modified cumulus parameterizations. There is a decrease in mean precipitation in the southeastern Pacific, suggesting that the MOD lessens the double ITCZ syndrome. The wet biases in the tropical Atlantic and western Africa are reduced but still larger than observed. The reduction of dry biases in the eastern Indian Ocean and equatorial Pacific are not significant. Over land, the dry biases in South America, central Africa, and South Asia decreased while wet biases in the central Africa and East Asia slightly increased. Compared with the MME of CMIP5, the horizontal pattern of the MOD is similar, while the magnitude of the biases is smaller, particularly in the tropical Pacific and western Indian Ocean. However, over land, the biases in North and

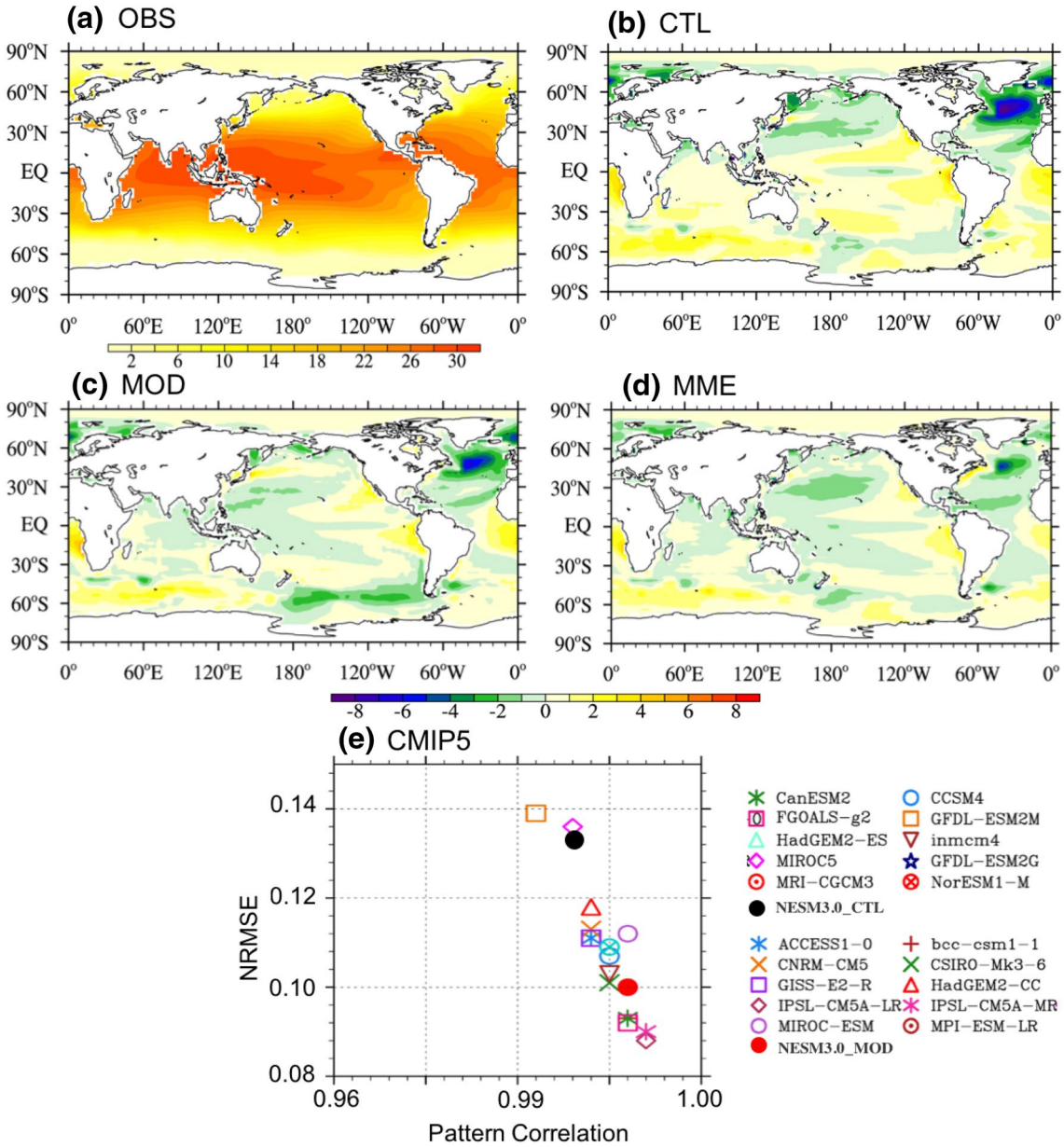

Fig. 3 Climatological mean SST (1979–2005) derived from **a** observation and biases simulated in **b** CTL, **c** MOD, and **d** MME of CMIP5 models. **e** CMIP5 models' performance on simulated climatological mean SST represented by pattern correlation coefficient and normalized root mean square error (NRMSE) in the global domain

South America are larger than the MME, suggesting that the major deficiency of the simulated precipitation from MOD occurs over the land regions. The range of pattern correlation and NRMSE in CMIP5 models is from 0.75 to 0.88 and 0.58 to 0.79, respectively. The models with better horizontal pattern tend to have smaller RMSEs.

Figure 7 shows biases in boreal summer and winter precipitation. In boreal summer, the CTL overestimates precipitation over the Maritime Continent, tropical Pacific and Atlantic ocean but underestimates it over the Indian Ocean, India, East Asia and Amazonian region. The MOD reduces wet biases over the tropical Pacific and Amazon butbdoes not improve it over the Indian Ocean. In boreal winter, the CTL overestimates precipitation over the Indian Ocean and Pacific but underestimates it in the Amazonian region. The MOD significantly reduces the wet biases in the Indian Ocean and Pacific.

The improved simulated SST and precipitation lead to better simulations of the atmospheric general circulation. The vertical profiles of annual mean temperature from observation and models are shown in Fig. 8. The CTL shows warm biases in the tropics from the BL to the upper

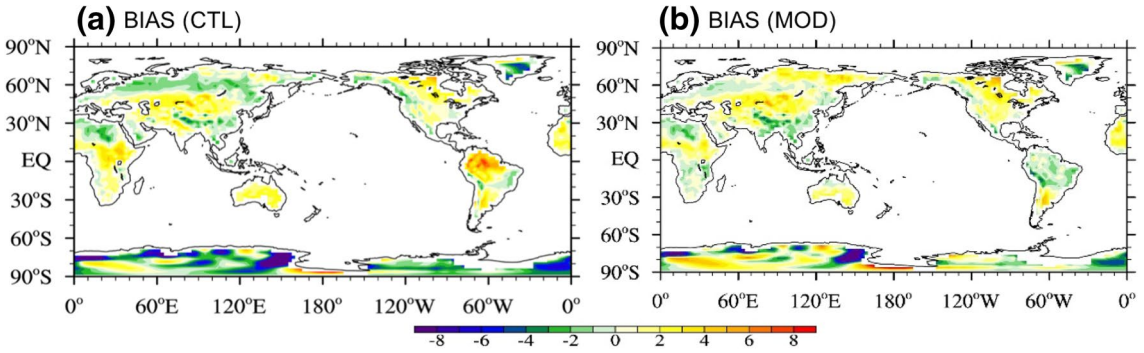

Fig. 4 Climatological mean SST (1979–2005) derived from biases simulated in **a** CTL and **b** MOD

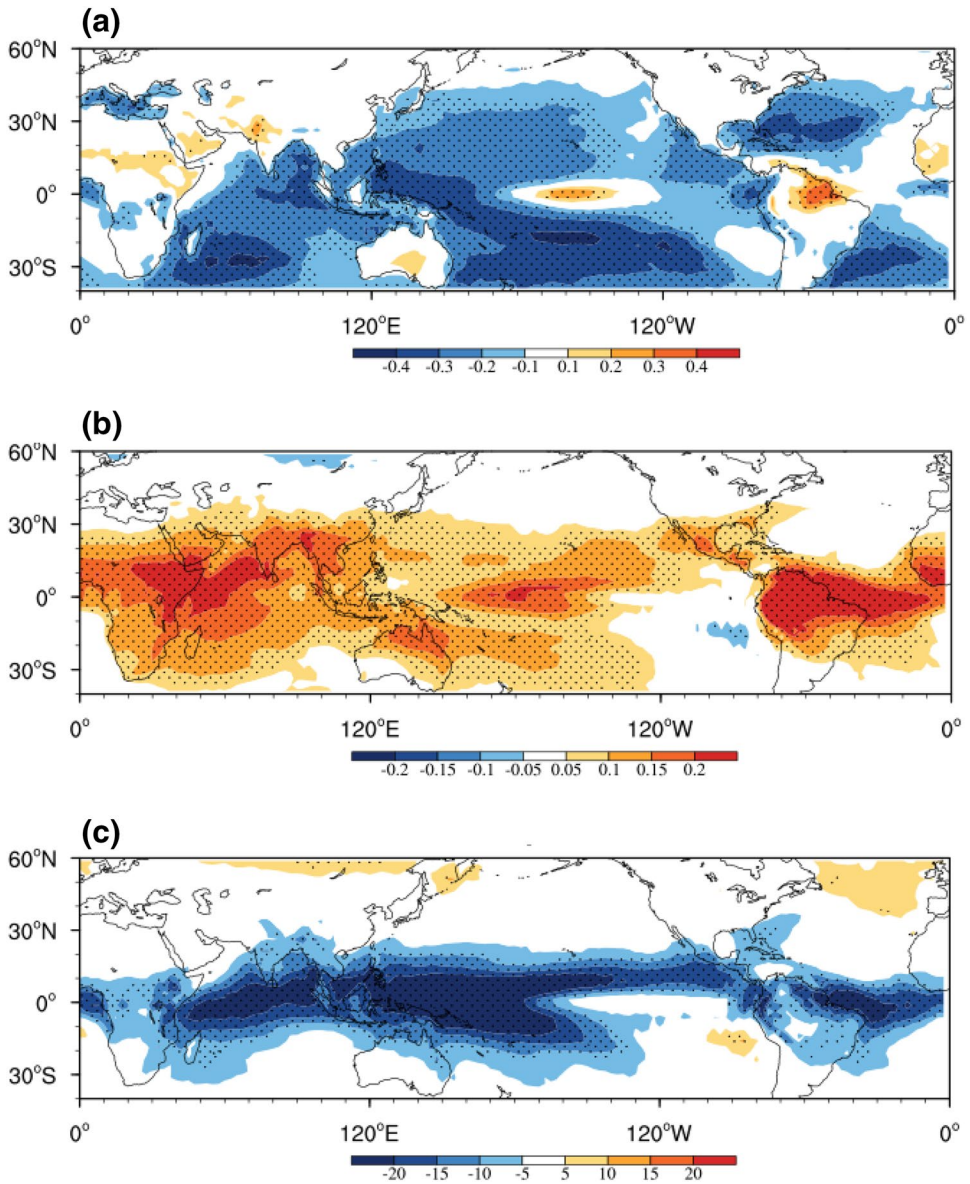

Fig. 5 Climatological difference of **a** ratio of convective to total precipitation, **b** total cloud cover and **c** net solar radiation at the surface between CTL and MOD (MOD minus CTL) during 1979–2005

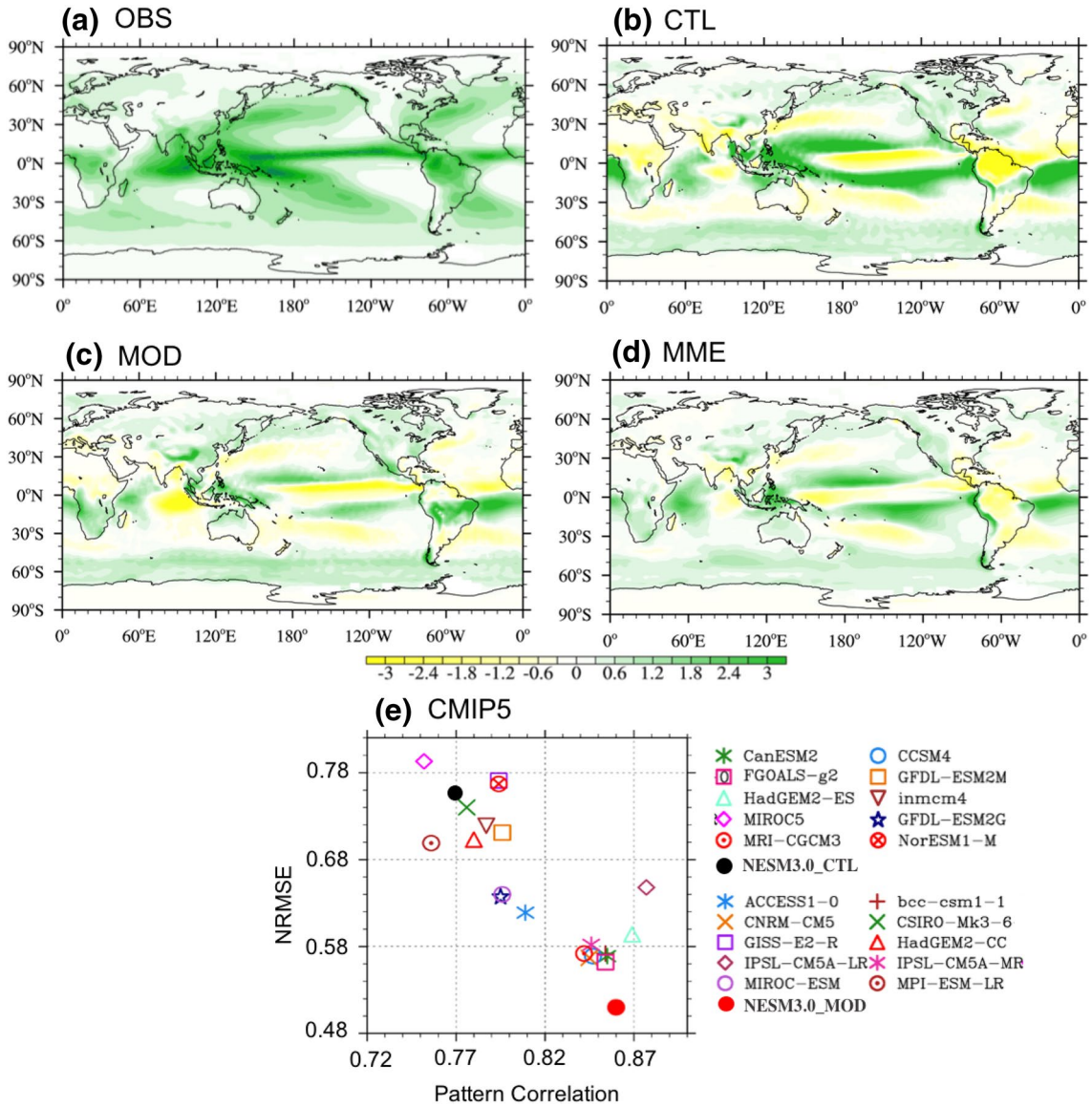

Fig. 6 The same as in Fig. 3 except for the climatological mean precipitation (1979–2005)

troposphere and cold biases in the middle and high latitudes at 200–300 hPa. The MOD improves vertical structure of temperature as seen from the reduced biases in the troposphere. The tropical warm biases decrease because deep convection tends to be suppressed by the modified parameterizations, which reduce vertical mixing and latent heating in the upper troposphere and cool the air there. The cold biases in high latitudes also decreased due to increased high cloudiness, which reduced radiative cooling. However, the cold biases in the tropical stratosphere are not reduced, which may be due to insufficient vertical resolution in the model's stratosphere. Polichtchouk et al. (2019) showed that cold biases of the stratosphere in a climate model may be reduced by increasing vertical resolution and/or better representation of gravity wave drag. Compared with the MME of CMIP5 models, the MOD simulates smaller cold biases in the upper troposphere and larger cold biases in the stratosphere. The range of pattern correlation (NRMSE) of the CMIP5 models is from 0.95 to 0.98 (0.22–0.40), suggesting that CMIP5 models capture the vertical structure of zonal temperature well but show a large spread for NRMSE.

Consistent with the improved temperature field, the vertical structure of zonal mean wind is also improved (Fig. 9). Observation shows a strong westerly jet near both 30° S and 30° N at 200 hPa. In the tropics, weak (strong) easterlies in the troposphere (stratosphere) are observed. The MOD reproduces the vertical structure of zonal wind reasonably well (Fig. 9c). Both the westerly biases in the midlatitude

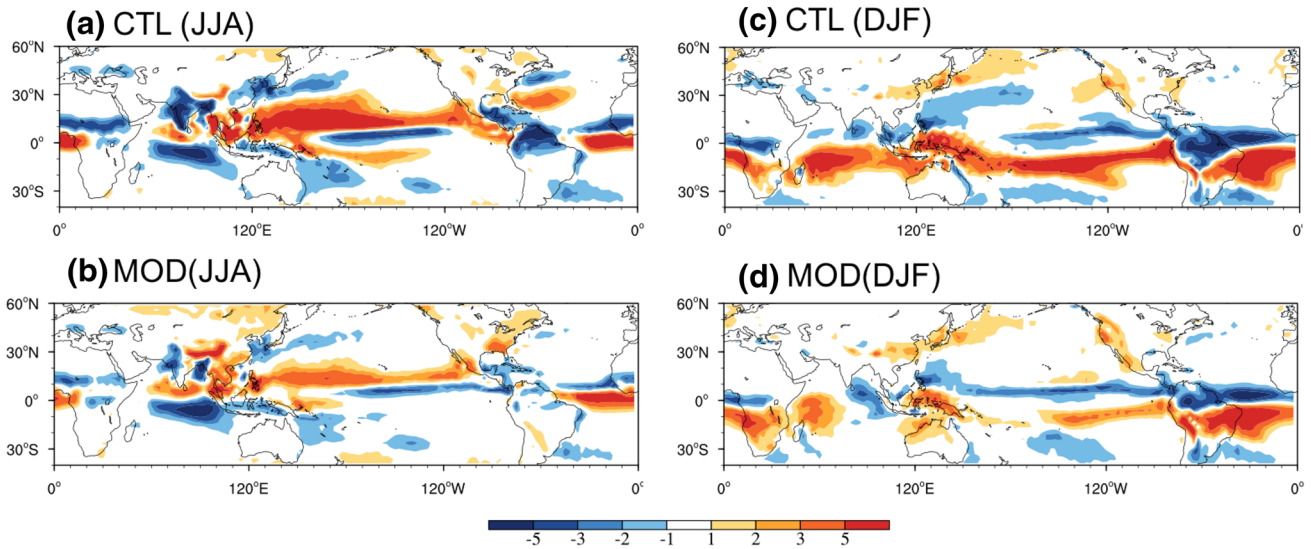

Fig. 7 Climatological seasonal mean precipitation (1979–2005) derived from biases simulated in CTL and MOD for boreal **a**, **b** summer and **c**, **d** winter

of upper troposphere and tropical stratosphere in the CTL (Fig. 9b) are reduced due to the lower meridional gradient of temperature in both hemispheres (Fig. 8c). The MME of CMIP5 has westerly biases in the upper troposphere and stratosphere in the southern Hemisphere and easterly biases in the tropical stratosphere due to strong meridional and vertical gradients of temperature there. In most regions, the MOD errors in simulated zonal wind tend to be smaller than those of the MME. The NRMSE of CMIP5 models are scattered from 0.22 to 0.4 but not for the pattern correlation.

In relation to the improved precipitation, the annual-mean sea surface salinity (SSS) showed significant improvement (Fig. 10). The CTL captures the horizontal pattern of the SSS well, however, it produces higher SSS in the Arctic and lower SSS in the North Atlantic, western Pacific, and coast of West Africa. The MOD reproduces the observed SSS pattern realistically except in the North Atlantic and Arctic region. The freshwater biases in the western Pacific and the coast of West Africa are reduced. Several factors may play a role in reduced freshwater biases in the tropics. In the improved freshwater fluxes, including better precipitation (Fig. 3) may be a dominant factor through reducing downward freshwater fluxes. In the CTL, the precipitation is overestimated over the western Pacific (e.g., Figure 3b) and SSS is underestimated (Fig. 10b). In the MOD, the precipitation in the western Pacific is reduced and SSS increased, which are both are closer to observations. This reduced freshwater flux may contribute to an increase in SSS. The increased surface easterly wind (Fig. 11) may contribute to the reduced SSS biases by freshwater advection. The CMIP5 models show relatively wide spreads for pattern correlation (0.74–0.95) and NRMSE (0.4–0.95).

The global monsoon (GM) is the dominant mode of annual variation and a defining feature of the Earth climate system (Wang and Ding 2008). The GM precipitation intensity is defined by the ratio of local summer-minus-winter precipitation to the annual total, thus reflecting the strength of the local summer precipitation and "monsoonality". The GM precipitation domain is defined by regions where the summer-minus-winter precipitation exceeds 2.5 mm day^{-1}, intensity exceeds 0.55 (Wang et al. 2011), and reflects the quality of the simulated seasonal distribution of the precipitation at each grid. Figure 12 shows that strong monsoon intensity is seen in South Asia and East Asia, western and eastern North Pacific, central and south Africa, and the Amazon basin. The MOD reduced the excessive intensity biases simulated in the CTL and improved the simulated monsoon precipitation domains by reducing the wet biases in the tropical Pacific, South Indian, and Atlantic oceans. Over land, the strong intensity bias of the CTL in Africa decreases in the MOD but the weak intensity bias in East Asia does not improve. The range of pattern correlation (NRMSE) of the CMIP5 models is from 0.72 to 0.83 (0.58–0.72), suggesting that many CMIP 5 models have a limited capacity to simulate GM intensity or the annual range of the precipitation.

4.3 Improved simulation of ENSO and PNA teleconnection

Figure 13 shows the spatial pattern of interannual variability of SST in the tropical Pacific. The observation shows maxima in the eastern Pacific and off the coast of South America. The CTL simulated excessive variability and the spatial location of the maximum extends westward. The

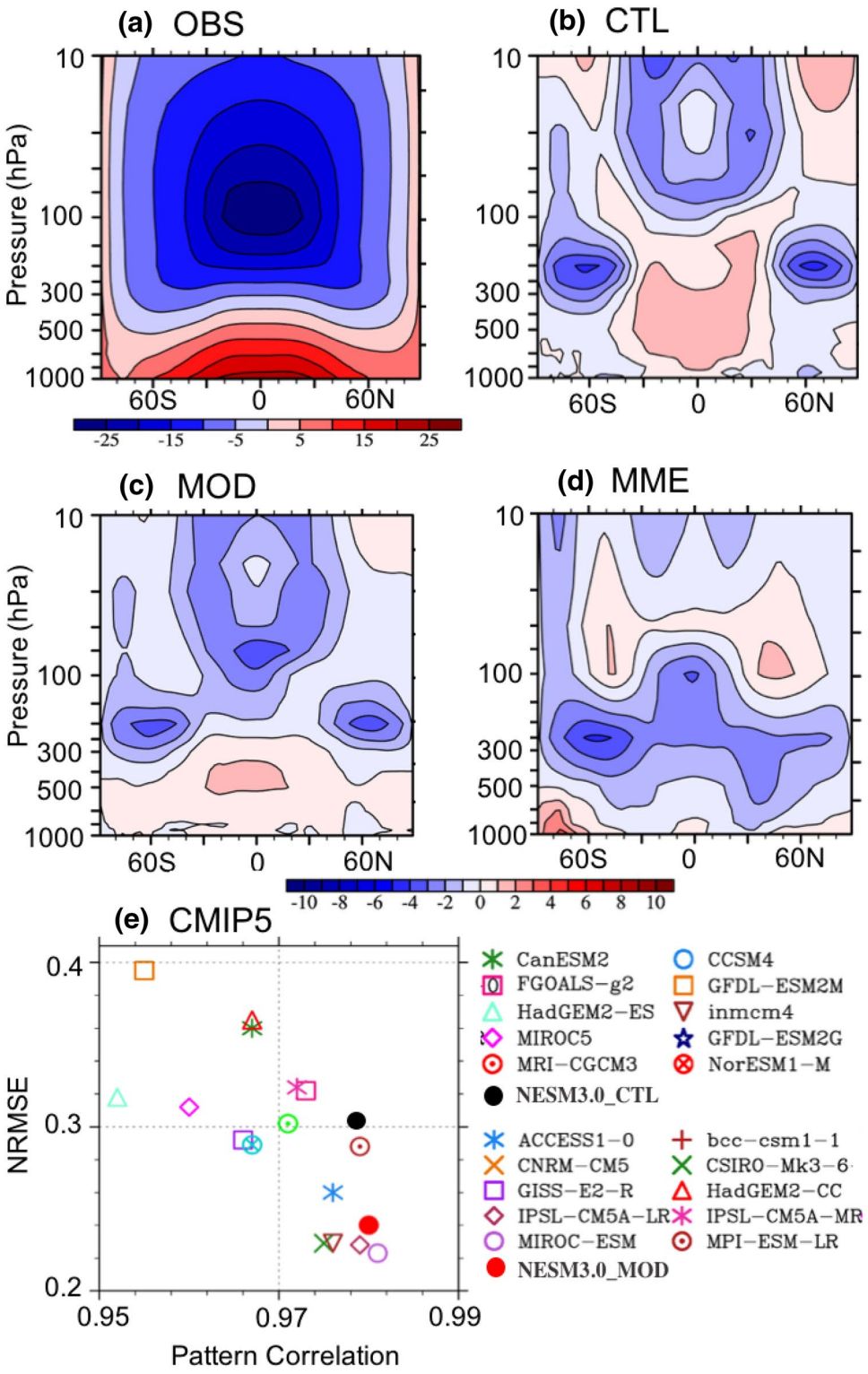

Fig. 8 Vertical structure of climatological zonal mean air temperature (1979–2005) from **a** observation and the biases simulated in **b** CTL, **c** MOD, and **d** MME of CMIP5 models. **e** CMIP5 models' performance on climatological air temperature represented by pattern correlation and NRMSE

MOD reproduces the horizontal pattern of the variability well except along the coastline of South America. The simulated magnitude of the variability is comparable to observation and the westward extension simulated in the CTL is almost removed in the MOD. The CMIP5 models show a significant spread for the pattern correlation (0.77–0.88) and large spread for NRMSE (0.54–1.10), which suggest that many CMIP5 models have biases in terms of the magnitude of the variability. Two possible reasons may contribute to the reduced interannual variability. In the MOD, the zonal

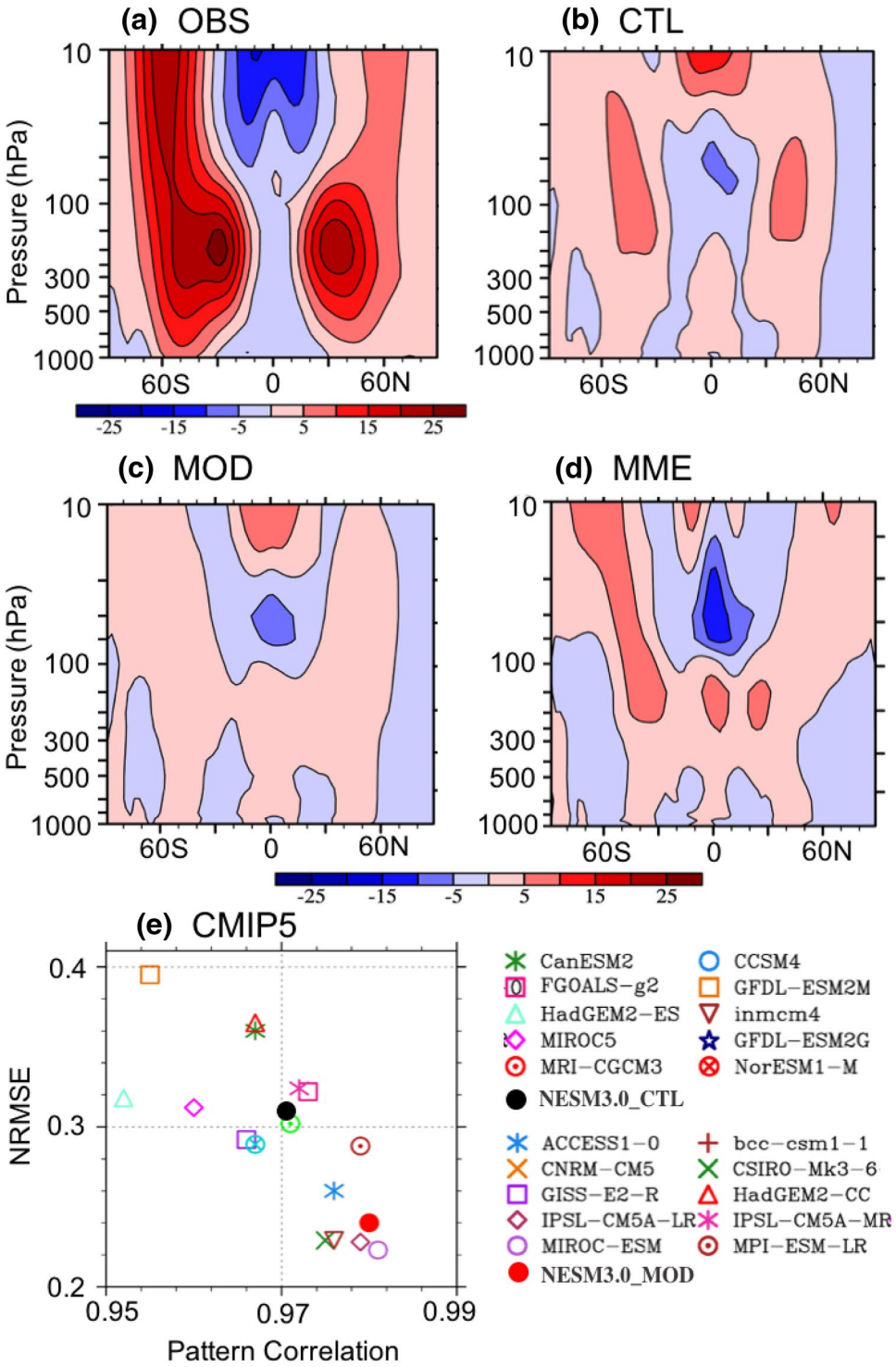

Fig. 9 The same as in Fig. 8 except for the vertical structure of climatological zonal mean zonal wind

gradients of the equatorial SST decrease due to the reduced western Pacific warming, which reduces advective feedback and thus the SST variability. The decreased mean precipitation in the eastern Pacific and the westward shift of wind stress anomalies associated with ENSO are also unfavorable for excessive strong El-Niño events. Figure 14 show zonal wind stress anomalies regressed on Nino 3.4 index. The observations show anomalous westerlies in the equatorial central Pacific and its peak is located near the date line. The westerly anomalies in the CTL are stronger and located slightly to the east compared to observations. In the MOD, the westerly anomalies are weakened and shift slightly westward compared to the CTL. The westerly anomalies associated with Nino3.4 index in MOD are improved with a higher

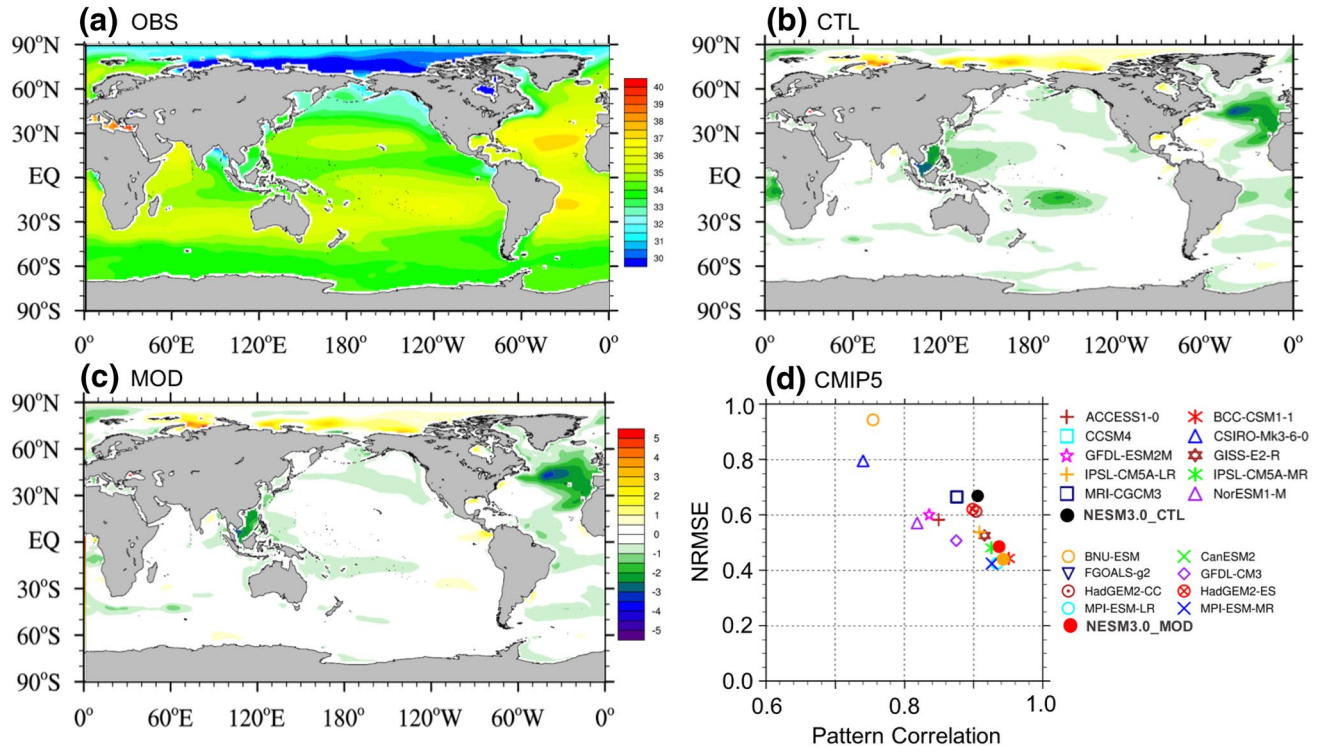

Fig. 10 The same as in Fig. 3 except for the climatological mean sue surface salinity (SSS)

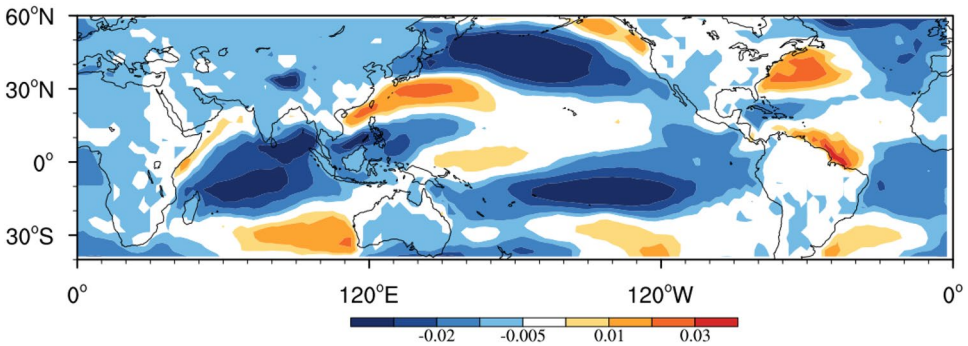

Fig. 11 Climatological difference of zonal wind stress between CTL and MOD (MOD minus CTL) during 1979–2005

pattern correlation of 0.87 and a lower normalized root mean square errors (NRMSE) of 0.68 when compared to those of CTL.

The power spectra of NINO3.4 SST are shown in Fig. 15. The observation shows a broad peak between 2 and 3 years and 4–5 years. The CTL captures the 2–3 year peak but shifts the 4–5 year peak to 5–7 years. The MOD captures the 4–5 year peak well and the 2–3 year peak is also simulated but slightly shorter. The ENSO phase locking to the seasonal cycle is an important feature (An and Wang 2001) but is missed in the CTL (Fig. 15d). The MOD simulation shows a similar phase locking to the observed counterpart (Fig. 15e), but the seasonal variation is significantly weaker. Moreover, the minimum NINO3.4 standard deviation in MOD is delayed by about 2 months with respect to observations.

Figure 16 shows the Pacific-North American teleconnection (PNA) patterns derived from the observation and model's simulations. The CTL captures the North Pacific trough but overestimates the ridge over western Canada and the trough over the Gulf of Mexico. The MOD captures more realistic Pacific trough and the ridge over western Canada as well as the trough over the Gulf of Mexico due to improved ENSO simulation. It is conceivable that the reduced ENSO variance and removal of its westward extension of the anomaly center may reduce the strong eastward extension of the ridge over western Canada and strong trough over the Gulf of Mexico by decreasing divergent flows over the eastern Pacific generated by ENSO. Figure 10d shows that about a half of CMIP5 models have difficulties in capturing realistic PNA patterns.

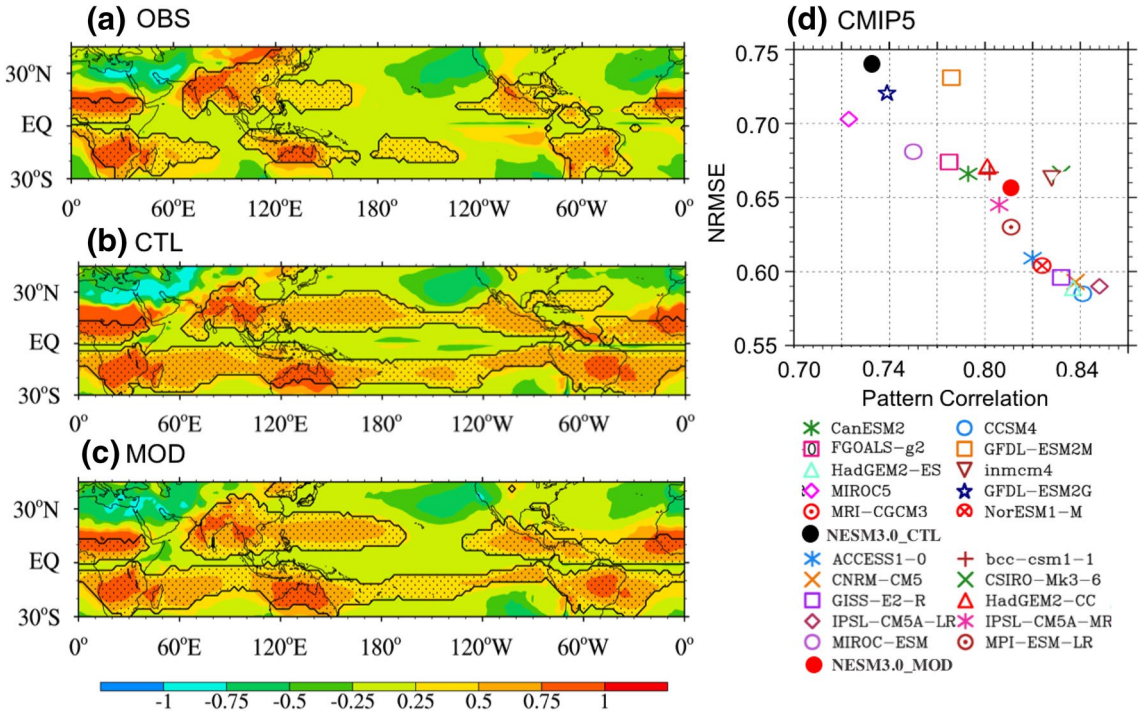

Fig. 12 Global monsoon domain (black line) and monsoon precipitation intensity (shading) (1979–2005) derived from **a** observed precipitation climatology, and the model **b** CTL and **c** MOD experiments. **d** CMIP5 models' performance on climatological global monsoon intensity represented by pattern correlation coefficient and NRMSE. The GM precipitation intensity is defined by the ratio of local Summer-minus-Winter precipitation to the annual total, where summer means May–September (MJJAS) for the NH and November–March (NDJFM) for the SH and winter means NDJFM for the NH and MJJAS for the SH. The GM precipitation domain is defined by the regions where the summer-minus-winter precipitation exceeds 2.5 mm day^{-1} and the GM precipitation intensity exceeds 0.55 (Wang et al. 2011)

4.4 Improved Madden–Julian oscillation (MJO)

The MJO is the dominant mode of intraseasonal variability of the tropical climate and the corner stone for subseasonal prediction. Figure 17 shows the observed lead-lag correlation of MJO precipitation with reference to the MJO precipitation centered at the eastern Indian Ocean (5° S–5° N, 80°–100° E). Both the MJO dry and wet precipitation events propagate eastward with a speed about 5 m s^{-1}. In CTL, very slow eastward propagation of precipitation is seen only in the Indian Ocean. However, with the modified parameterization, the model simulates the systematic eastward propagation of the MJO from the Indian Ocean to western Pacific, indicating that the modified parameterizations significantly improve the MJO simulation. The CMIP5 models show a large spread for the pattern correlation (0.43–0.93) and NRMSE (0.36–0.82), which suggest that CMIP5 models' performance in MJO simulation vary considerably.

Theories and climate model diagnostics suggest that boundary layer moisture convergence (BLMC) feedback plays an important role in eastward propagation MJO precipitation. Observation shows that the BLMC propagates eastward systematically from 50° E to 180° E and the propagation of precipitation is led by the BLMC by about 5 days (Fig. 18a). The CTL failed to capture the propagation of BLMC but the MOD reproduces realistic eastward propagation of the BLMC, which leads the convection propagation. The improvement is due to the use of the BL depth-dependent convective trigger function and the enhanced interaction between the BL moisture convergence and the lower tropospheric heating in the shallow convection scheme (Yang and Wang 2019). The performance of CMIP5 models in simulating BLMC propagation was measured by the pattern correlation and NRMSE score between the observations and simulations in the domain of (−20 to +20 day and 50° E–180° E). Figure 18d shows a large diverse pattern correlation from 0.3 to 0.89 and NRMSE from 0.45 to 0.94. Compared to Fig. 17d, the model with better propagation of MJO precipitation tends to have better pattern correlations for propagation of BLMC, suggesting that enhanced BLMC feedback is closely associated with better MJO simulation.

Figure 19 shows the MJO circulation structure at the lower troposphere (850 hPa). Observation shows that the MJO has a coupled Rossby–Kelvin wave structure with the MJO major convection in the Indian Ocean. The equatorial maximum westerly speed associated with the Kelvin wave

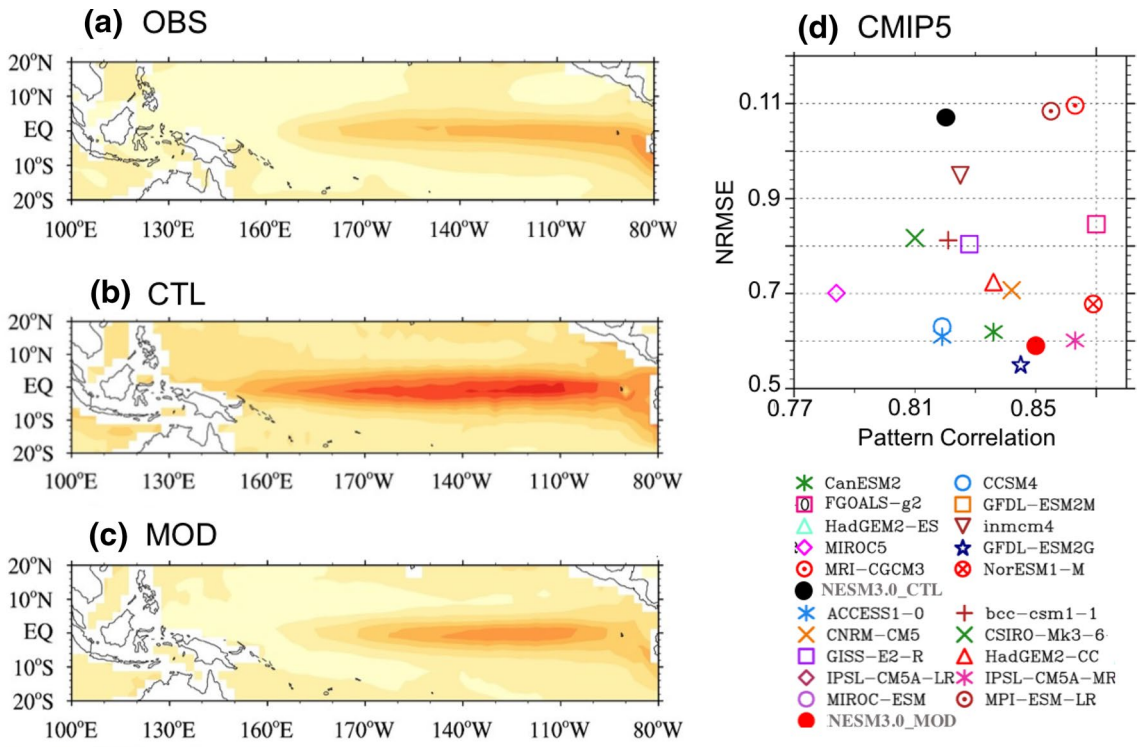

Fig. 13 Interannual variance of SST anomalies (1950–2005) derived from **a** observation, **b** CTL, and **c** MOD. **d** CMIP5 models' performance on simulation of the interannual SST variance represented by pattern correlation coefficient and NRMSE

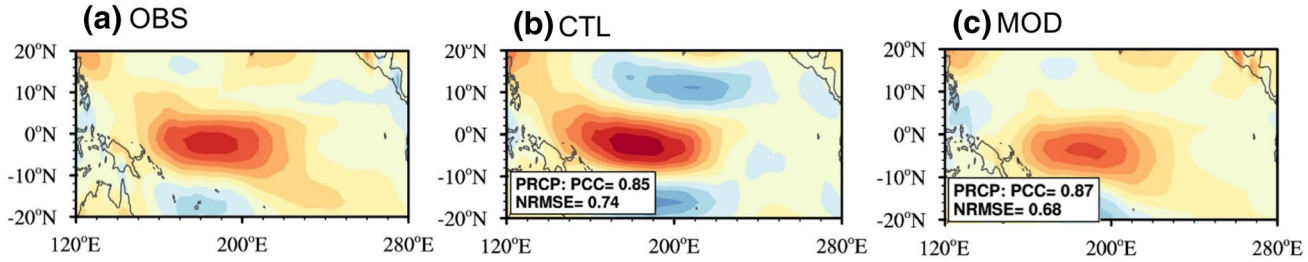

Fig. 14 Zonal wind stress anomalies regressed onto Niño-3.4- averaged SST anomalies, all months included (mPa $°C^{-1}$) from the observations and models. Observations are regressed onto the ERSST V4 for 1979–2014, and correspond to stress anomalies from ERA-Interim data

response in the MJO is slightly weaker than the maximum easterly speed (1:1.2). The horizontal circulation pattern simulated in the CTL is different from that of the observed MJO: the zonal wind is not symmetric about the equator and the westerly to the west of the MJO center is stronger than the easterly to the east of the MJO center (Fig. 19b). In contrast, the MOD experiment produces circulation patterns that are much more similar to the observed ones. The equatorial maximum westerly speed in the MJO is comparable with the maximum easterly speed (1:1.05). On the other hand, the intensity of the maximum Kelvin wave easterly is stronger than the observation, suggesting that MJO propagation speed may be higher than the observation For fast propagation speed of the simulated MJO from MOD may be due to stronger Kelvin wave response (e.g., Wang et al. 2018).

5 Conclusion

In this study a suite of climate model simulations was conducted to improve a historical run. The earlier version of NESM3.0 produces reasonable trends of global mean temperature and energy balance but the simulated climatology and climate variability have significant deficiencies, including the warm SST bias in the tropics and associated excessive precipitation, double ITCZ, unrealistic ENSO and MJO, as well as PNA teleconnection patterns (Sect. 3.1).

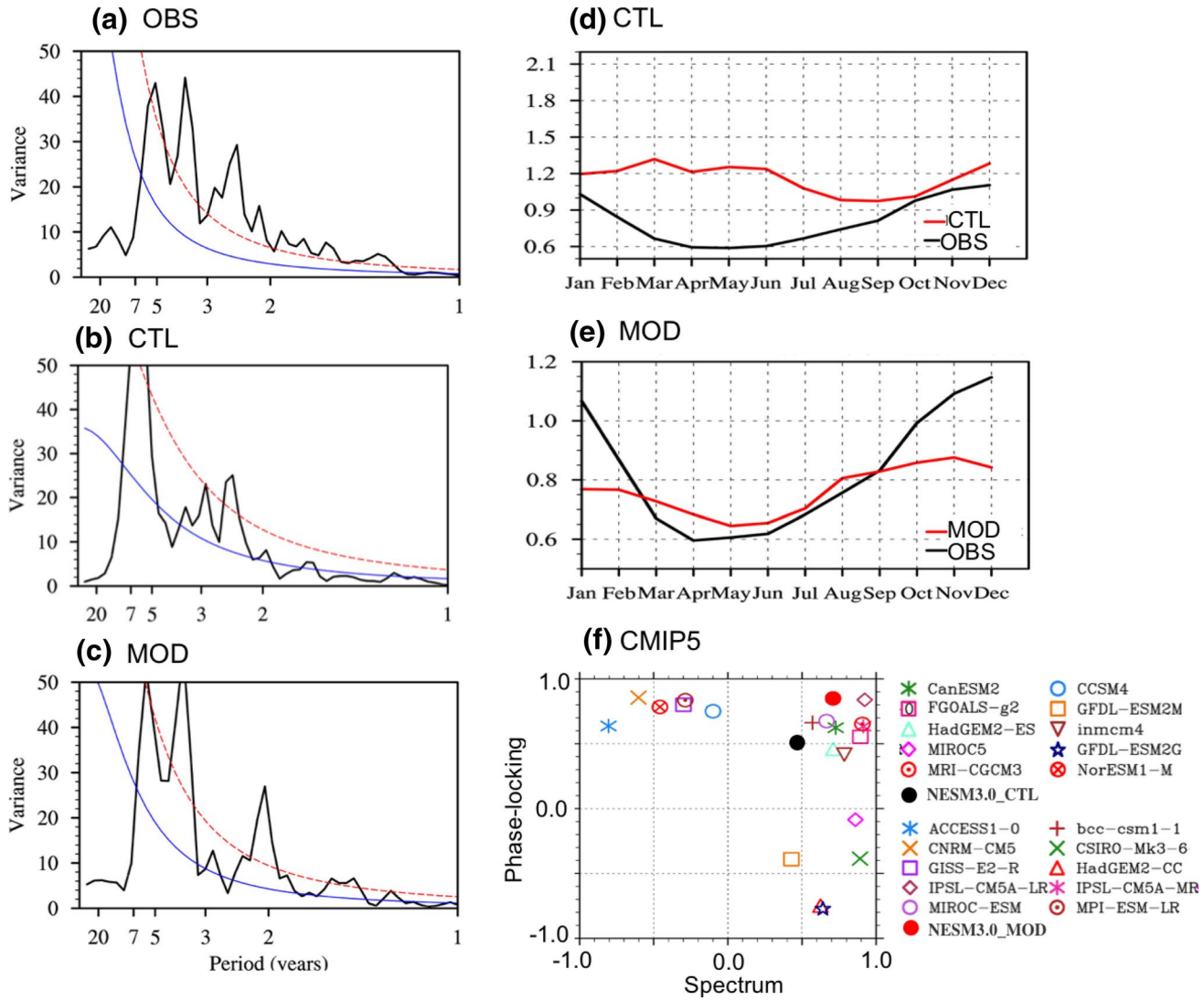

Fig. 15 Power spectrum of the NINO3.4 SST anomalies (1950–2005) derived from **a** observation, **b** CTL, and **c** MOD. Seasonality of the interannual variance of NINO3.4 SST anomalies from **d** CTL and **e** MOD. **f** CMIP5 models' performance on ENSO represented by pattern correlation coefficients of power spectrum and seasonality (phase-locking)

To improve model climatology and variability without degrading global energy balance, modified parameterization schemes were implemented in the NESM3.0. The major modifications include improved deep and shallow convection schemes, cloud cover, and cloud microphysics scheme (Sect. 3.2).

The results show that the NESM3.0 with modified parameterizations improves simulated climatology and climate variability in its historical run without degrading global energy balance. The key fields improved are the SST and precipitation climatology. The MOD reduces warm SST bias and excessive precipitation biases significantly by suppressing convective precipitation. The model also reduces temperature biased in the tropical upper troposphere due to reduced vertical mixing. The improved mean state in precipitation and SST and circulation can contribute to better GM by reducing monsoon intensity in the western Pacific, whereas the CTL produces too strong monsoon and warm SST biases. In the ocean, salinity in the western Pacific is improved by reducing precipitation and reducing easterly wind in the eastern Pacific. Over land, the warm bias is reduced by increasing cloudiness.

The MOD improves major modes of climate variability. The eastward propagation of the MJO is improved by enhancing shallow convection ahead of deep MJO convection and interaction between the boundary layer and lower tropospheric heating. The ENSO amplitude of the MOD is improved by reducing the zonal wind stress and precipitation associated with SST anomalies. The phase lock of ENSO to seasonal cycle is well reproduced, which may be due to the modified

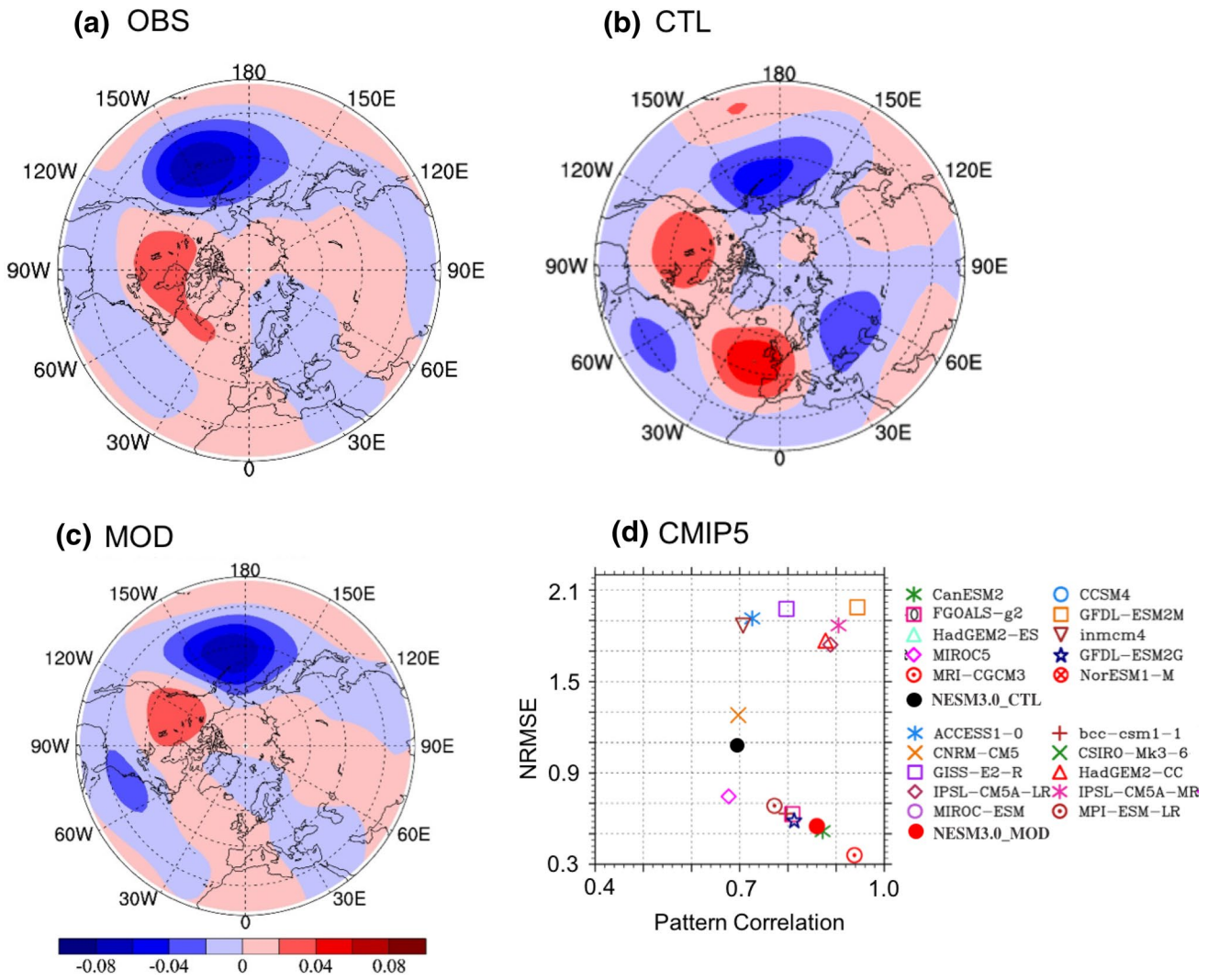

Fig. 16 Regression of 200 hPa heights onto standardized NINO3.4 SST anomalies for the DJF season (1979–2005) from **a** observation, **b** CTL, and **c** MOD. **d** CMIP5 models' performance on simulation of PNA pattern-by-pattern correlation coefficient and NRMSE

convective scheme. The PNA pattern is much improved by improved ENSO simulation.

It is expected that other coupled climate models, which suffer similar systematic biases as the earlier version of NESM, may benefit from the application of the modified parameterizations proposed in this work. It would be interesting to see to what extent they are useful and study model-dependent results due to modification of the moist physical parameterizations. The modified parameterization may affect other CMIP6 runs such as abrupt 4CO2 run and AMIP run. We plan to investigate their sensitivities in future studies.

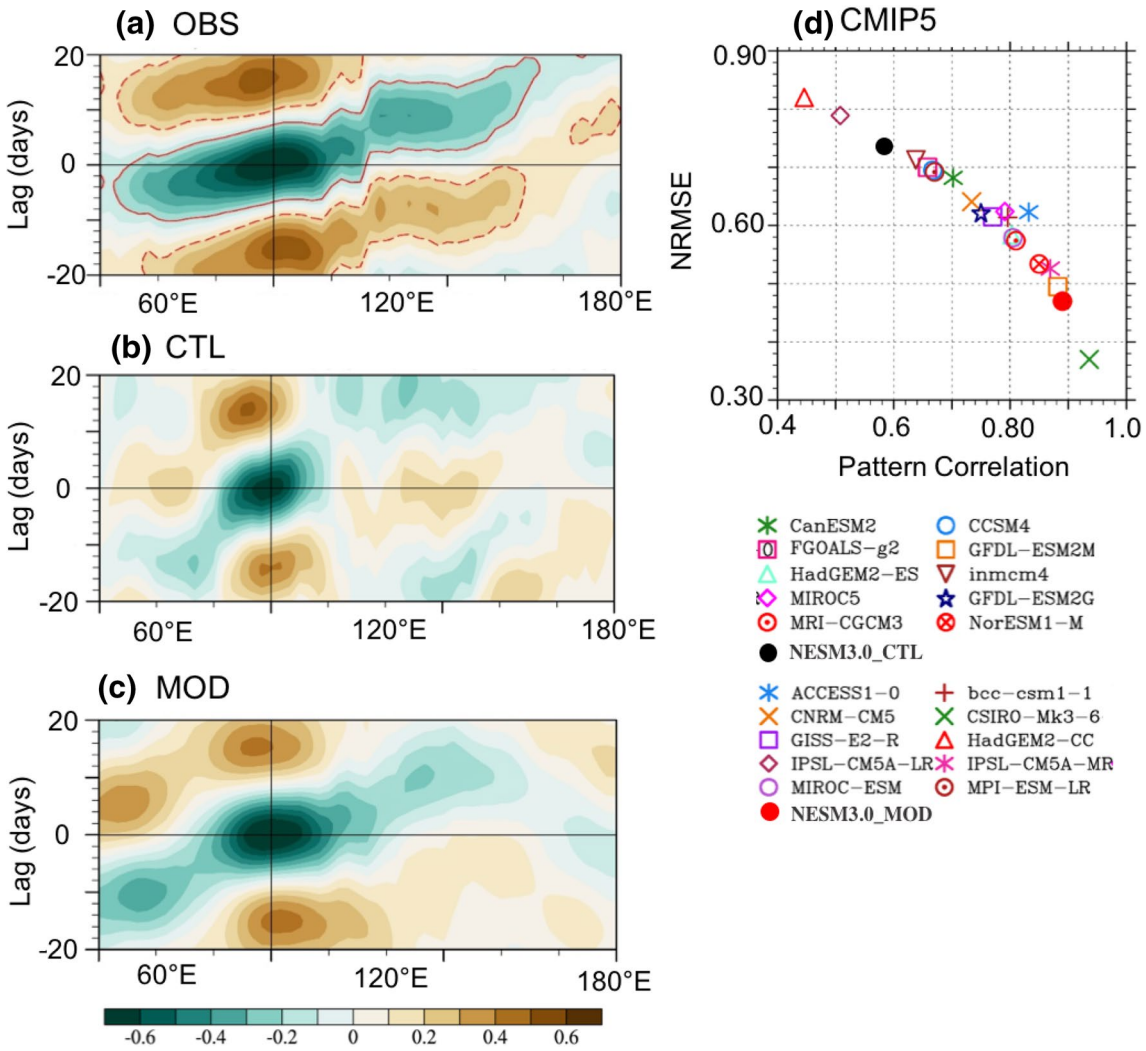

Fig. 17 Lagged correlation of 20–70 days filtered precipitation averaged over 10 S–10 N with reference to the precipitation in the eastern Indian Ocean (80–100 E, 10 S–10 N) during boreal winter (NDJFMA) from **a** observation, **b** CTL, and **c** MOD. **d** CMIP5 model's performance on MJO precipitation propagation represented by pattern correlation coefficient and NRMSE. The red contour represents the correlation coefficient of 0.2. The black vertical and horizontal lines show 90 E and lag of 0 day

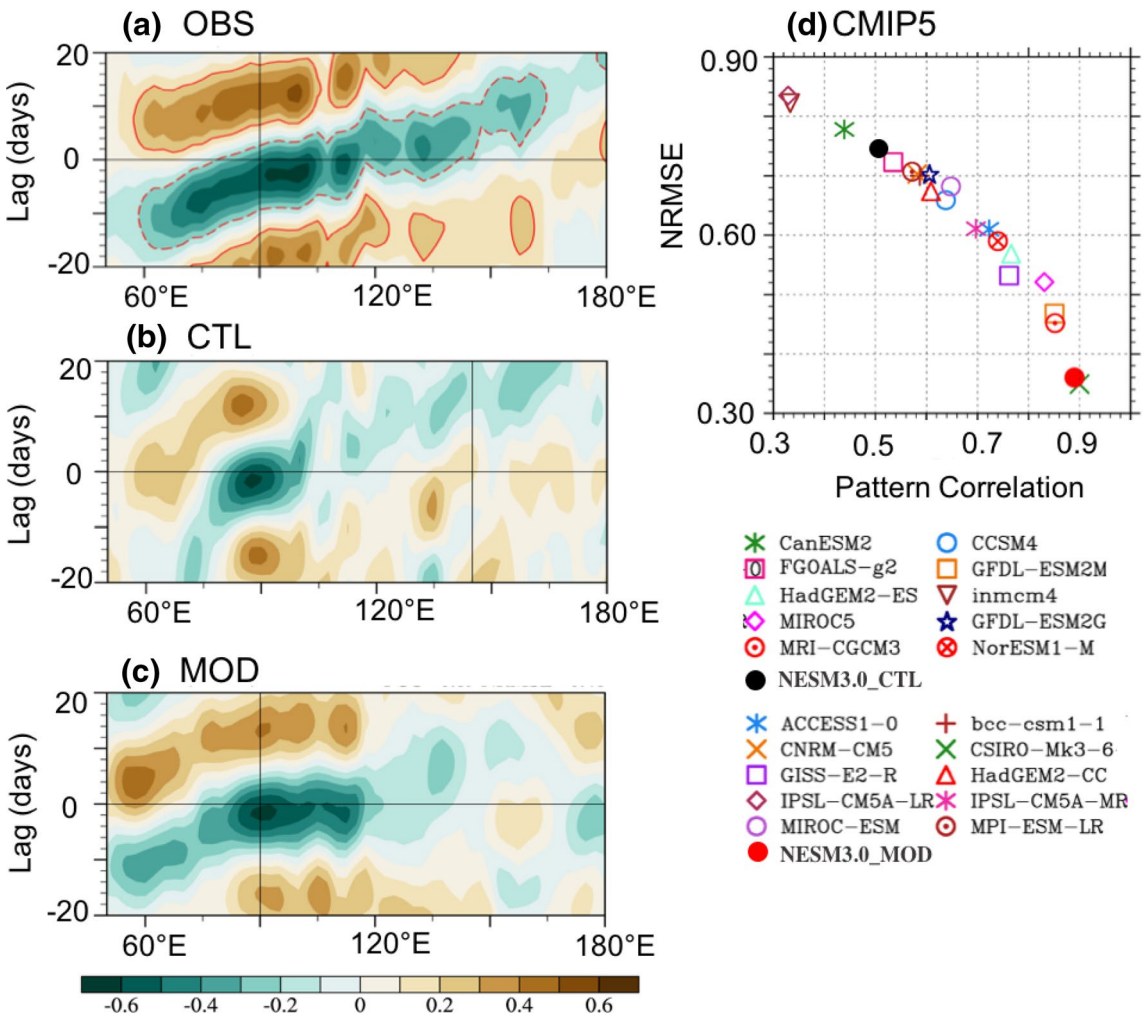

Fig. 18 The same as in Fig. 11 except for the 20–70 days filtered boundary layer moisture convergence

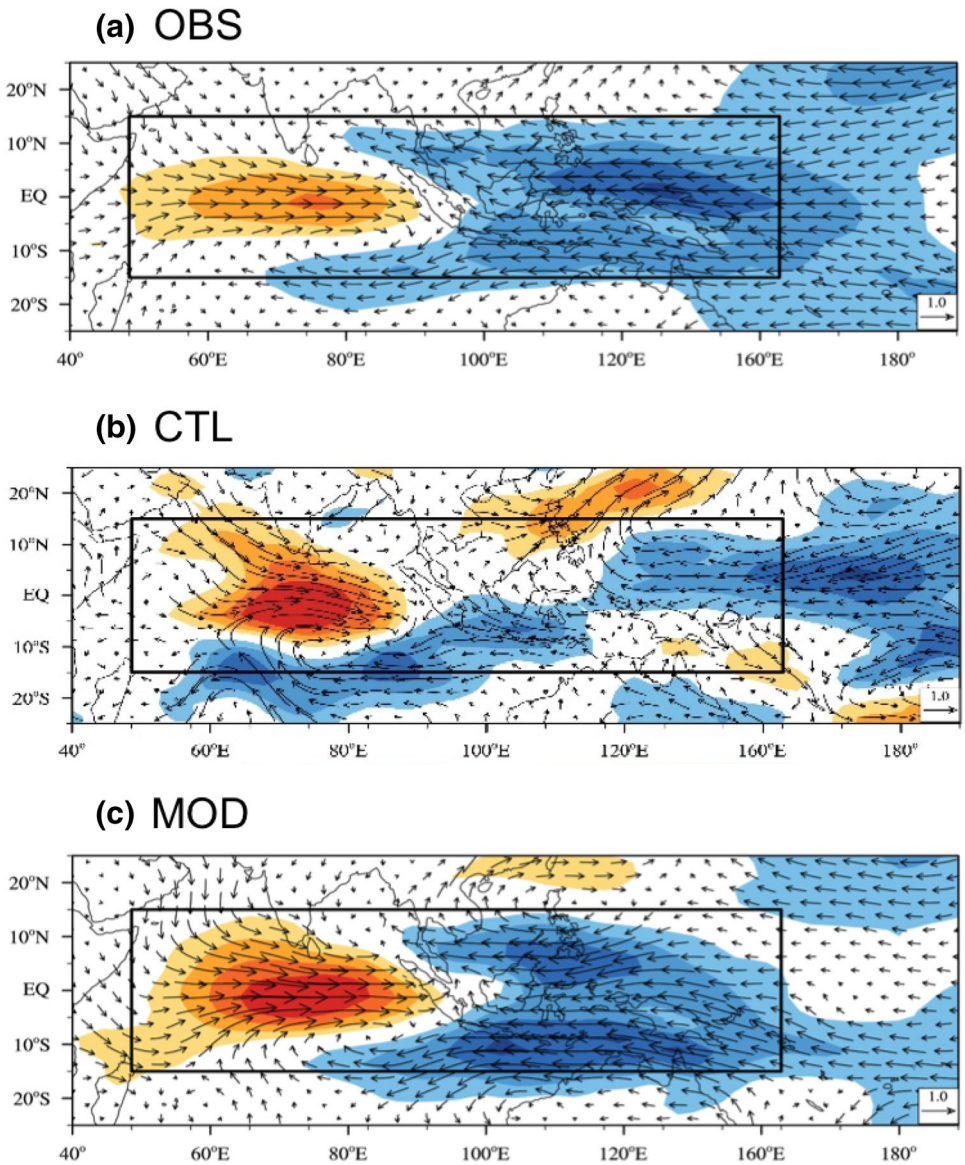

Fig. 19 The MJO circulation structure at 850 hPa. Horizonal structure of horizontal wind (unit: m s^{-1}, vector) and zonal wind speed (unit: m s^{-1}, shading) at 850 hPa depicted by the regressed 20–70-day filtered wind onto the 20–70-day filtered precipitation averaged over the MJO precipitation center (10° S–10° N, 80°–100° E) obtained from **a** observation and model simulations with **b** CTL and **c** MOD during boreal winter (November–April). The regression strengths are scaled to a fixed 3 mm day^{-1} precipitation rate

References

Adler RF et al (2003) The version-2 global precipitation climatology project (GPCP) monthly precipitation analysis (1979–present). J Hydrometeorol 4(6):1147–1167

An S-I, Wang B (2001) Mechanisms of locking the El Niño and La Niña mature phases to boreal winter. J Clim 14:2164–2176

Balmaseda MA, Mogensen K, Weaver AT (2013) Evaluation of the ECMWF ocean reanalysis system ORAS4. Q J R Meteorol Soc 139:1132–1161

Beard KV (1976) Terminal velocity and shape of cloud and precipitation drops aloft. J Atmos Sci 33:851–864

Beard K, Pruppacher HR (1969) A determination of the terminal velocity and drag of small water drops by means of a wind tunnel. J Atmos Sci 26:L066–L1072

Beheng KD (1994) A parameterization of warm cloud microphysical conversion processes. Atmos Res 33:193–206

Cao J, Wang B, Yang Y-M, Ma L, Li J, Sun B, Bao Y, He J, Zhou X (2018) The NUIST earth system model (NESM) version 3: description and preliminary evaluation. Geosci Model Dev Discuss 1:2975–2993

Chen C et al (2017) ENSO in the CMIP5 simulations: life cycles, diversity, and responses to climate change. J Clim 30:775–801

Dee DP et al (2011) The ERA-Interim reanalysis: configuration and performance of the data assimilation system. Q J R Meteorol Soc 137(656):553–597

Ham YG, Kug JS, Kim D, Kim YH, Kim DH (2013) What controls phase-locking of ENSO to boreal winter in coupled GCMs? Clim Dyn 40:1551–1568

Huang B, Thorne PW, Smith TM, Liu W, Lawrimore J, Banzon VF, Zhang H-M, Peterson TC, Menne M (2016) Further exploring and quantifying uncertainties for extended reconstructed sea surface temperature (ERSST) version 4 (v4). J Clim 29:3119–3142

Hung M-P, Lin J-L, Wang W, Kim D, Shinoda T, Weaver SJ (2013) MJO and convectively coupled equatorial waves simulated by CMIP5 climate models. J Clim 26:6185–6214

Kanamitsu M, Ebisuzaki W, Woollen J, Yang SK, Hnilo JJ, Fiorino M, Potter GL (2002) NCEP-DOE AMIP-II reanalysis (R-2). Bull Am Meteorol Soc 83:1631–1643

Kang I, Yang Y, Tao W (2014) GCMs with implicit and explicit representation of cloud microphysics for simulation of extreme precipitation frequency. Clim Dyn 45:325–335. https://doi.org/10.1007/s00382-014-2376-1

Kim D, Kang IS (2012) A bulk mass flux convection scheme for climate model: description and moisture sensitivity. Clim Dyn 38:411–429. https://doi.org/10.1007/s00382-010-0972-2

Kim D, Jang Y-S, Kim D-H, Kim Y-H, Watanabe M, Jin F-F, Kug J-S (2011) El Niño-Southern Oscillation sensitivity to cumulus entrainment in a coupled general circulation model. J Geophys Res 116:D22112

Kumar S, Merwade V, Kinter JL, Niyogi D (2013) Evaluation of temperature and precipitation trends and long-term persistence in CMIP5 twentieth-century climate simulations. J Clim 26:4168–4185

Langleben MP (1954) The terminal velocity of snowflakes. Q J R Meteorol Soc 80:171–181

Lee Y-Y, Black RX (2013) Boreal winter low-frequency variability in CMIP5 models. J Geophys Res Atmos 118:6891–6904

Lee J-Y, Wang B, Kang IS, Shukla J, Kumar A, Kug JS, Schemm JKE, Luo JJ, Yamagata T, Fu X, Alves O (2010) How are seasonal prediction skills related to models performance on mean state and annual cycle? Clim Dyn 35:267–283

Li G, Xie S-P (2012) Origins of tropical-wide SST biases in CMIP multi-model ensembles. Geophys Res Lett 39:L22703

Li J, Yang Y-M, Wang B (2018) Evaluation of NESMv3 and CMIP5 models' performance on simulation of Asian–Australian monsoon. Atmosphere 9:327

Madec G et al (2008) NEMO ocean engine. IPSL Tech, Note, p 332

Meehl GA, Boer GJ, Covey C, Latif M, Stouffer RJ (2000) The Coupled Model Intercomparison Project (CMIP). Bull Am Meteorol Soc 81:313–318

Meehl GA, Teng H, Arblaster JM (2014) Climate model simulations of the observed early-2000s hiatus of global warming. Nat Clim Change 4:898–902

Möbis B, Stevens B (2012) Factors controlling the position of the intertropical convergence zone on an aquaplanet. J Adv Model Earth Syst 4(4):M00A04

Nordeng TE (1994) Extended versions of the convective parametrization scheme at ECMWF and their impact on the mean and transient activity of the model in the tropics. European Centre for Medium-Range Weather Forecasts

Perovich DK, Tucker WB III (1997) Arctic sea ice conditions and the distribution of solar radiation during summer. Ann Glaciol 25:445–450

Perovich DK, Grenfell TC, Light B, Hobbs PV (2002) Seasonal evolution of the albedo of multiyear Arctic sea ice. J Geophys Res 107:8044. https://doi.org/10.1029/2000JC000438

Polichtchouk I, Coauthors (2019) Control on stratospheric temperature in IFS: resolution and vertical advection, ECMWF technical Meomoranda. https://www.ecmwf.int/sites/default/files/elibrary/2019/19084-control-stratospheric-temperature-ifs-resolution-and-vertical-advection.pdf

Raddatz TJ, Coauthors (2007) Will the tropical land biosphere dominate the climate–carbon cycle feedback during the twenty-first century? Clim Dyn 29:565–574

Shu Q, Song Z, Qiao F (2015) Assessment of sea ice simulations in the CMIP5 models. Cryosphere 9:399–409

Stevens B et al (2013) Atmospheric component of the MPI-M earth system model: ECHAM6. J Adv Model Earth Syst 5(2):146–172

Stroeve JC et al (2012) Trends in Arctic sea ice extent from CMIP5, CMIP3 and observations. Geophys Res Lett 39:L16502

Taylor KE, Stouffer RJ, Meehl GA (2012) An overview of CMIP5 and the experiment design. Bull Am Meteorol Soc 93(4):485–498

Tiedtke M (1989) A comprehensive mass flux scheme for cumulus parameterization in large-scale models. Month Weather Rev 117(8):1779–1800

Tiedtke M et al (1988) Tropical forecasting at ECMWF: the influence of physical parameterization on the mean structure of forecasts and analyses. Q J R Meteorol Soc 114(481):639–664

Valcke S, Coauthors (2013) OASIS3-MCT user guide, OASIS3-MCT 2.0. CERFACS/CNRS SUC URA (1875)

Wang B, Ding QH (2008) Global monsoon: dominant mode of annual variation in the tropics. Dyn Atmos Oceans 44:165–183

Wang B, Lee S-S (2017) MJO propagation shaped by zonal asymmetric structures: results from 24-GCM simulations. J Clim 30(19):7933–7952

Wang B, Kim HJ, Kikuchi K, Kitoh A (2011) Diagnostic metrics for evaluation of annual and diurnal cycles. Clim Dyn 37:941–995

Wang B, Liu F, Chen G (2016) A trio-interaction theory for Madden–Julian oscillation. Geosci Lett 3:34. https://doi.org/10.1186/s40562-016-0066-z

Wang B, Lee S-S, Waliser DE et al (2018) Dynamics-oriented diagnostics for the Madden–Julian Oscillation. J Climate 30:3743–3769

Watanabe M, Chikira M, Imada Y, Kimoto M (2011) Convective control of ENSO simulated in MIROC. J Clim 24:543–562

Yanai M, Esbensen S, Chu J-H (1973) Determination of bulk properties of tropical cloud clusters from large-scale heat and moisture budgets. J Atmos Sci 30:611–627

Yang Y-M, Wang B (2019) Improving MJO simulation by enhancing the interaction between boundary layer convergence and lower tropospheric heating. Clim Dyn 52(7–8):4671–4693

Yang YM, Wang B, Li J (2018) Improving seasonal prediction of East Asian summer rainfall using NESM3.0: preliminary results. Atmosphere 9:487

Yang Y-M, Wang B, Lee J-Y (2019a) Mechanisms of northward propagation of boreal summer intraseasonal oscillation revealed by climate model experiments. Geophys Res Lett. https://doi.org/10.1029/2018GL081612

Yang Y-M, Lee J-Y, Wang B (2019b) The Tibetan Plateau uplift is crucial for eastward propagation of Madden–Julian Oscillation. Sci Rep 9:15478

Yang Y-M, An S-I, Wang B, Park JH (2019c) A global-scale multidecadal variability driven by Atlantic multidecadal oscillation. Nat Sci Rev (accepted)

Zhang GJ, Song XL (2009) Interaction of deep and shallow convection is key to Madden–Julian oscillation simulation. Geophys Res Lett 36:L09708